

ABSTRACT

KWON, HYEOKJUN. RF Signal Source Search and Localization Using an Autonomous UAV. (Under the direction of Dr. Ismail Guvenc).

Advancements in unmanned aerial vehicle (UAV) technology have led to their increased utilization in various commercial and military applications. One such application is signal source search and localization (SSSL) using UAVs, which offers significant benefits over traditional ground-based methods due to improved RF signal reception at higher altitudes and inherent autonomous 3D navigation capabilities. Localization of a radio frequency (RF) signal source has various use cases, ranging from search and rescue, identification and deactivation of jammers, and tracking hostile activity near borders or on the battlefield. However, the limited flight duration of UAVs due to battery constraints, as well as limited computational resources on board of lightweight UAVs introduce challenges for SSSL. In this thesis, we study various SSSL techniques using a UAV with predefined waypoints. A linear least square (LLS) based localization scheme is considered with enhanced reference selection due to its relatively lower computational complexity.

In Chapter 2, given the free space path loss propagation model, five different LLS localization algorithms are proposed and studied for selecting anchor positions to be used for localization as the UAV navigates through an area. The performance of each algorithm is measured in two ways: 1) real-time positioning accuracy during the ongoing UAV flight, and 2) long-term accuracy measured at the end of the UAV flight. We compare and analyze the performance of the proposed approaches using computer simulations in terms of accuracy, UAV flight distance, and reliability.

In Chapter 3, we adopt a two-ray channel model and a dipole antenna pattern to develop a simulator that more closely represents real-world radio signal strength (RSS) observations at a

UAV. We then examine and compare the performance of previously proposed linear least square (LLS) based localization techniques using UAVs for SSSL. Localization of radio frequency (RF) signal sources is assessed based on two main criteria: 1) achieving the highest possible accuracy and 2) localizing the target as quickly as possible with reasonable accuracy. Our results show that use of more realistic propagation and antenna models may significantly affect the localization performance.

© Copyright 2023 by HYEOKJUN KWON

All Rights Reserved

RF Signal Source Search and Localization Using an Autonomous UAV

by
HYEOKJUN KWON

A thesis submitted to the Graduate Faculty of
North Carolina State University
in partial fulfillment of the
requirements for the Degree of
Master of Science

Electrical and Computer Engineering

Raleigh, North Carolina
2023

APPROVED BY:

Dr. Mihail Sichertiu

Dr. Ozgur Ozdemir

Dr. Ismail Guvenc
Chair of Advisory Committee

DEDICATION

To my family and MPACT Lab.

BIOGRAPHY

The author was born in Seoul, South Korea. He started studying at the Korea Military Academy in 2009. He got his Bachelor's degree in Military Management from there in 2013. In the same year, he became a South Korean army officer. He worked in many different roles in the Army. In 2021, he decided to go back to school. He began a Master's degree in Computer Engineering at NC State University. In the summer of 2022, he started working as a student at the MPACT Lab. He did his thesis research there under the guidance of Dr. Ismail Guvenc.

ACKNOWLEDGEMENTS

This thesis was made possible by the generous support of the National Science Foundation (NSF) under grant number CNS-1939334. I am deeply thankful to the South Korean Army for allowing and supporting me in my studies at NC State University. I owe immense gratitude to my advisor, Dr. Ismail Guvenc. His careful guidance and continuous support were invaluable to my work. I also wish to express my sincere thanks to my committee members, Dr. Mihail Sichitiu and Dr. Ozgur Ozdemir. Dr. Sichitiu broadened my understanding and experience in the fields of UAV and autonomous systems. Simultaneously, Dr. Ozdemir played a crucial role in helping me familiarize myself with the AERPAW project and its experiments. Lastly, I cannot overstate the impact of my family on my academic journey. My wife, Hyeseung, and my lovely son, Hyogyem, were my greatest supporters. Their constant love and encouragement were instrumental in the completion of this work.

TABLE OF CONTENTS

List of Tables	vi
List of Figures	vii
Chapter 1 INTRODUCTION	1
1.1 Literature Review	2
1.2 Contribution of this Thesis	3
Chapter 2 RF SSSL Using an Autonomous UAV with Free Space Path Loss Model	5
2.1 System Model	5
2.2 Proposed SSSL Methods	9
2.2.1 LLS-CON	10
2.2.2 LLS-CUM	11
2.2.3 LLS-FML	11
2.2.4 LLS-CHLM	12
2.2.5 LLS-CLS	12
2.2.6 Performance Analysis Criteria	13
2.3 Measurement Results and Anlysis	15
2.3.1 Localization Performance for Fixed Target Location	16
2.3.2 Average Localization Accuracy	16
Chapter 3 RF SSSL by an Autonomous UAV with Two-Ray Channel Model and Dipole Antenna Patterns	21
3.1 System Model	21
3.2 Proposed SSSL Methods	26
3.3 Measurement Results and Anlysis	28
3.3.1 Analysis of RSS for Different Scenarios	30
3.3.2 Analysis of Distance Estimation Accuracy	31
3.3.3 Analysis of Proposed SSSL Methods	36
Chapter 4 Conclusions and Future work	43
References	45

LIST OF TABLES

Table 2.1	Summary of parameters for generic LLS algorithm in the free space path loss model.	8
Table 2.2	SSSL algorithms performance summary in the free space path loss model.	17
Table 3.1	Summary of simulation parameters in the two-ray propagation model. . .	29
Table 3.2	SSSL algorithms performance summary in the two-ray propagation model.	38

LIST OF FIGURES

Figure 2.1	SSSL for ground target localization using an autonomous UAV with predefined waypoints in the free space path loss model.	7
Figure 2.2	Five different SSSL algorithms considered in the free space path loss model.	14
Figure 2.3	Parallel track pattern for SSSL with a UAV.	15
Figure 2.4	Comparison of SRL and DRL for a fixed target location considering five different SSSL approaches and their variations in the free space path loss model.	18
Figure 2.5	RMSE of five different SSSL approaches and their variations averaged over different target locations in the free space path loss model.	19
Figure 2.6	CDF of RMSE averaged over different target locations in the free space path loss model.	20
Figure 3.1	Two-ray propagation model.	23
Figure 3.2	SSSL algorithms considered in the two-ray propagation model.	26
Figure 3.3	Trajectory of the UAV with fixed waypoints, and three different signal source locations that the UAV is searching in the two-ray propagation model. While all the target locations are on the ground, their corresponding locations at the UAV's altitude are also illustrated, to show their relative location with respect to the UAV's trajectory more clearly. . . .	30
Figure 3.4	RSS measurements for various scenarios in the two-ray propagation model: RSS vs. distance.	31
Figure 3.5	RSS measurements for various scenarios in the two-ray propagation model: RSS vs. trajectory.	32
Figure 3.6	Distance estimation RMSE for distance variation in the two-ray propagation model.	33
Figure 3.7	Distance estimation RMSE for angle variation in the two-ray propagation model.	34
Figure 3.8	Location estimation RMSE for distance variation in the two-ray propagation model.	35
Figure 3.9	Location estimation RMSE for angle variation in the two-ray propagation model.	36
Figure 3.10	Localization RMSE comparison upon on-target locations in the two-ray propagation model: Omni, Dipole (with altitude 30m, 50m, and 70m) .	39
Figure 3.11	Localization RMSE comparison upon mid-target locations in the two-ray propagation model: Omni, Dipole (with altitude 30m, 50m, and 70m) .	40
Figure 3.12	Localization RMSE comparison upon far-target locations in the two-ray propagation model: Omni, Dipole (with altitude 30m, 50m, and 70m) .	41

Figure 3.13 CDFs of the localization error and localization time for different techniques and scenarios in the two-ray propagation model. 42

CHAPTER

1

INTRODUCTION

The availability of unmanned aerial vehicles (UAVs) has expanded in various industries, leading to rapid growth in the UAV market. As interest in the UAV industry continues to increase, numerous studies and experiments are being conducted aggressively. Especially compared to ground systems, UAVs have significant advantages in achieving line of sight. In addition, UAVs offer flexibility in deployment for various situations with immediate response time. These characteristics make UAVs well-suited for signal source searching and localization (SSSL) missions. Based on this, received signal strength based localization schemes with UAV is studied in [1, 2].

1.1 Literature Review

From a high-level perspective, we can categorize the UAV localization requirements into two: 1) localization accuracy with fixed flight time (LAFFT): requiring a high localization accuracy, and 2) localization time with fixed localization accuracy (LTFLA): demanding fast localization with a coarse accuracy. For example, the implementation of UAVs for positioning hostile targets with RF signals in warfare is studied in [3, 4]. In addition, positioning a GPS jammer in an open area is investigated in [5]. These are representative examples of LAFFT because accurate localization is highly critical for a precise strike in warfare. On the other hand, the localization, search, and rescue of victims (e.g., after disasters) in an undetermined vast area within a limited time is studied in [6, 7, 8]. This can be categorized as LTFLA since the localization time may be more critical than achieving a very low localization accuracy.

In this context, a wide range of studies aiming to improve UAV-based localization performance are available in the literature. For example, finding the optimal UAV trajectory for a given area or figuring out the better formation of UAVs for localization have been studied in the past. In [9], various UAV search patterns and their traits are summarized. Trajectory design for localizing a source signal with an unmanned mini-helicopter is investigated based on a Moore space-filling curve algorithm in [10]. The importance of optimizing UAV search patterns for improving localization accuracy is explored in [11, 12]. In another recent study, a group of small UAVs performs radio frequency positioning with flexible and practical formations in [13].

In addition, statistical approaches to improve localization accuracy are extensively explored. In [14], localization and tracking algorithms based on an extended Kalman filter are analyzed. Parallel with this, particle filter-based localization algorithms are investigated and compared with an extended Kalman filter algorithm in [15, 16]. In addition, localizing a node based on particle filter is studied in [17]. The effect of the unknown path loss exponent on localization

performance is studied in [18, 19]. In addition, The dependence of the localization accuracy on the transmitter and receiver's antenna patterns are quantified in [20, 21].

Recently, machine learning (ML) based localization algorithms have been getting attention for better performance of UAV-based SSSL. In [22], a Q-Learning-based positioning algorithm is suggested to localize illegal radio stations. Similar to this, source signal-based Q-learning scheme for UAV navigation is studied in [23].

However, the aforementioned algorithms may require a high computational complexity, which may not be feasible for lightweight UAVs with limited batter and computational capacities. Moreover, existing ML-based approaches typically require prior training of the ML technique in the same environment which may not always be possible. In this sense, the computation complexity of various localization algorithms is studied in a broader sense in [24]. Furthermore, efforts to reduce the computational complexity of UAV based localization are conducted by converting the nonlinear and non-convex problems into linear and convex problems in [25].

1.2 Contribution of this Thesis

While UAV-based SSSL techniques have been investigated in the literature, there are still various research challenges to be addressed. While some SSSL use cases may prioritize accuracy at the cost of longer search time, some other use cases may require a rough location estimate but need it quickly and at low computational complexity. In this context, In Chapter 2, the main contributions are listed as follows:

- Five approaches are proposed for anchor point selection over a UAV's trajectory to carry out linear least squares (LLS)-based real-time target localization;
- Accuracy, latency, reliability, and complexity of the five LLS-based localization techniques

are compared using computer simulations;

- Two methods for selecting the linearization reference point are compared for LLS: i) static reference selection (SRL) that uses the first point of the UAV trajectory as the reference point, and ii) dynamic reference selection (DRL) that uses the reference point dynamically.

In Chapter 2, a simple propagation model was used for simplicity. In Chapter 3, we adopt more realistic antenna and propagation models and evaluate the localization performance under such models. Based on this, the main contributions of Chapter 3 are listed as follows:

- Rather than the free-space propagation assumption in Chapter 2, we use the two-ray propagation model that may to some extent characterize air-to-ground propagation in an open field.
- We consider both omnidirectional and doughnut-shaped dipole antenna patterns with different UAV altitudes for performance analysis.
- We evaluate a modified version of the SSSL algorithms in Chapter 2 and compare their localization accuracy and localization time for various scenarios.

CHAPTER

2

RF SSSL USING AN AUTONOMOUS UAV WITH FREE SPACE PATH LOSS MODEL

2.1 System Model

In this chapter, we consider the problem of RF SSSL of a target node on the ground using a single autonomous UAV as illustrated in Fig. 2.1. In particular, a UAV flies autonomously on a path with predefined waypoints and its goal is to localize the target node as quickly and as accurately as possible. To do that, the UAV has to select anchor points for continuously estimating the target's location as it moves through its trajectory. As more observations are

obtained, localization accuracy is expected to improve. However, using all reference points over the UAV's trajectory does not necessarily provide the best accuracy, as will be shown using computer simulations.

The propagation channel model for UAV network is typically assumed to have a line of sight (LOS) with the signal source, which we also assume in this chapter for simplicity. For an LOS path, accurate distance estimation is possible because path loss mainly depends on the distance between the UAV and the transmitter [26]. Considering LOS and open space, free-space path loss (FSPL) model is used to calculate the estimated distance between the target node and the UAV, given by [27]:

$$\text{PL}(d) = \text{PL}_0 + 10\alpha \log_{10} \left(\frac{d}{d_0} \right) + X_\sigma, \quad (2.1)$$

where PL_0 is the path loss at the reference distance d_0 , α denotes the path loss exponent in the free space that is set to be 2 in this work, X_σ is a Gaussian random variable with mean zero and standard deviation σ to capture shadowing effects, and d is the distance between the ground target and the UAV. Using (2.1), the distance \hat{d}_i with the ground target node can be estimated at the i th UAV flight location and it can then be expressed as follows [28]:

$$\hat{d}_i = f_i(x, y, z) + n_i, \quad i = 1, \dots, \tilde{N}, \quad \tilde{N} = 1, \dots, N, \quad (2.2)$$

where n_i is the white noise at the i th UAV location, \tilde{N} is the index for the current location of the UAV, N is the index of the last location at the end of the UAV's trajectory, and $f_i(x, y, z)$ is the real distance between the target (x, y, z) and the i th UAV location (x_i, y_i, z_i) . This can be described as [28]

$$f_i(x, y, z) = \sqrt{(x - x_i)^2 + (y - y_i)^2 + (z - z_i)^2}. \quad (2.3)$$

With the estimated distance \hat{d}_i obtained at multiple UAV reference points, the least squares

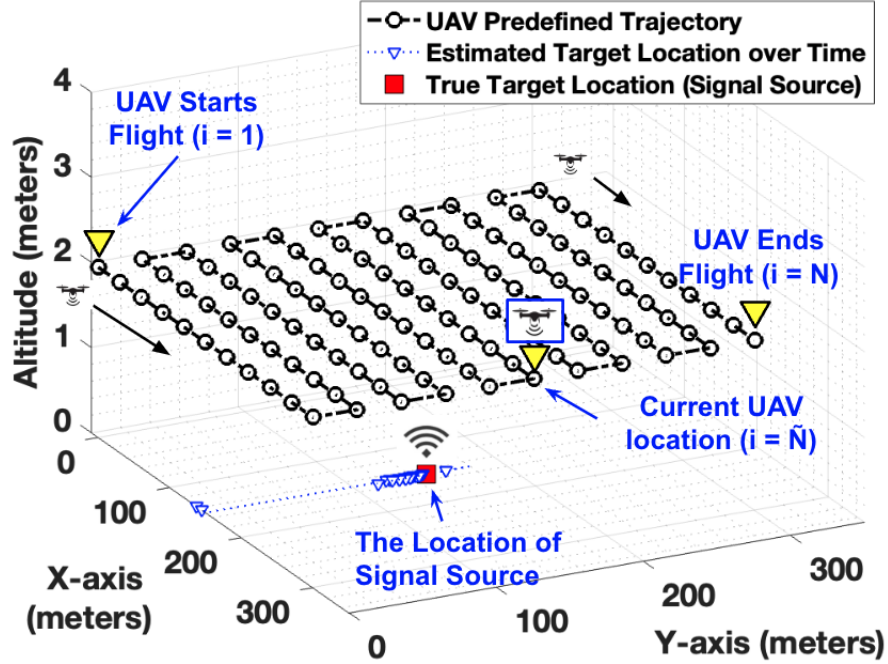


Figure 2.1: SSSL for ground target localization using an autonomous UAV with predefined waypoints in the free space path loss model.

(LS) algorithm can be effectively used for both linear and nonlinear parameter estimation. However, due to the high computational complexity of the nonlinear least square algorithm [28], we consider an LLS-based localization technique in this study. In the LLS algorithm, a set of linear equations are obtained based on simple mathematical combinations of equations (2.2) and (2.3). In particular, (2.2) and (2.3) can be expressed (neglecting noise terms) as follows for $i = 1, \dots, \tilde{N}$ [29]

$$d_i^2 = (x - x_i)^2 + (y - y_i)^2 + (z - z_i)^2 . \quad (2.4)$$

Localization of the ground target requires distance estimates to the target measured at a minimum of three different UAV anchor positions. We define the index set v of size $3 \leq S \leq \tilde{N}$ that captures the unique UAV indices (anchor positions) to be used in the localization process. Details of how to form v will be discussed further in the next section.

Table 2.1: Summary of parameters for generic LLS algorithm in the free space path loss model.

Parameters	Stands for
i	UAV flight index
N	The index at the end of the UAV trajectory
\tilde{N}	The UAV index at the current location
\mathcal{v}	a set of UAV indices used for LLS algorithm
S	Size of index array \mathcal{v}
k	Elements index in \mathcal{v}

For LLS-based localization, we have to set the r th index, $r \in \mathcal{v}$, as a reference index for localization. Two methods are suggested for selecting the linearization reference. With the SRL mode, the first index of \mathcal{v} is selected as the reference. On the other hand, in DRL mode, indices in the \mathcal{v} are sorted in ascending order, and the index with the smallest distance (between the target and the UAV) is adopted as the reference. This reference selection scheme is used for all the suggested LLS schemes in Section 2.2.

After selecting the reference for linearization, the reference equation (corresponding to \hat{d}_r in (2.2)) is subtracted from all the other equations corresponding to the set \mathcal{v} , which can be written in matrix notation as follows for $k = 1, \dots, S$, and $k \neq r$ [28, 29]

$$A_{\mathcal{v}}l = b_{\mathcal{v}}, \quad (2.5)$$

where $l = [\hat{x}, \hat{y}, \hat{z}]^T$ is the estimated target location,

$$A_v = 2 \begin{bmatrix} x_{v(1)} - x_r & y_{v(1)} - y_r & z_{v(1)} - z_r \\ \vdots & \vdots & \vdots \\ x_{v(k)} - x_r & y_{v(k)} - y_r & z_{v(k)} - z_r \\ \vdots & \vdots & \vdots \\ x_{v(S)} - x_r & y_{v(S)} - y_r & z_{v(S)} - z_r \end{bmatrix}, \quad (2.6)$$

and

$$b_v = \begin{bmatrix} d_r^2 - d_{v(1)}^2 + x_{v(1)}^2 + y_{v(1)}^2 + z_{v(1)}^2 - \lambda \\ \vdots \\ d_r^2 - d_{v(k)}^2 + x_{v(k)}^2 + y_{v(k)}^2 + z_{v(k)}^2 - \lambda \\ \vdots \\ d_r^2 - d_{v(S)}^2 + x_{v(S)}^2 + y_{v(S)}^2 + z_{v(S)}^2 - \lambda \end{bmatrix}, \quad (2.7)$$

where λ is $(x_r^2 + y_r^2 + z_r^2)$ and $v(k)$ is k th index of v . The estimated target location l is given using LLS as [28, 29]

$$l = (A_v^T A_v)^{-1} A_v^T b_v. \quad (2.8)$$

2.2 Proposed SSSL Methods

Based on the system model in Section 2.1, in this section we propose and evaluate five different approaches for dynamically forming and updating the index set v as the UAV moves along its trajectory. In particular, we study five different approaches: 1) Consecutive three-point (CON); 2) Cumulative all-points (CUM); 3) First-mid-last points (FML); 4) Convex hull modified (CHLM); and 5) Closest three-points (CLS). Each algorithm considers different approaches for obtaining anchors and the reference UAV positions to populate the matrix A_v in (2.6). After the

anchors are selected for the current location \tilde{N} of the UAV, LLS based localization is carried out with SRL or DRL as described in the previous section.

2.2.1 LLS-CON

The main idea of the LLS-CON is to use the minimum relative residual, where the relative residual is defined as:

$$R_{\tilde{N}} = \frac{\|b_{\mathbf{v}} - A_{\mathbf{v}}l\|}{\|b_{\mathbf{v}}\|}, \quad (2.9)$$

where $\|\cdot\|$ returns the L_1 norm of its argument, and l is the estimated target location with LLS localization based on the UAV index array \mathbf{v} . In this algorithm, three consecutive points are used as anchor locations in \mathbf{v} for SSSL. In particular, the index array \mathbf{v} is defined as follows:

$$\mathbf{v} = \begin{cases} \{\tilde{N}, \tilde{N} - 1, \tilde{N} - 2\}, & \text{if } R_{\tilde{N}} \leq R_{\tilde{N}-1} \\ \{\tilde{N} - 1, \tilde{N} - 2, \tilde{N} - 3\}, & \text{otherwise} \end{cases}.$$

Two modified versions of LLS-CON are also considered that leave larger gaps between consecutive UAV locations. In particular, \mathbf{v} for LLS-CON-I is defined as

$$\mathbf{v} = \begin{cases} \{\tilde{N}, \tilde{N} - 2, \tilde{N} - 4\}, & \text{if } R_{\tilde{N}} \leq R_{\tilde{N}-1} \\ \{\tilde{N} - 1, \tilde{N} - 3, \tilde{N} - 5\}, & \text{otherwise} \end{cases},$$

while for LLS-CON-II, \mathbf{v} is defined as

$$\mathbf{v} = \begin{cases} \{\tilde{N}, \tilde{N} - 3, \tilde{N} - 6\}, & \text{if } R_{\tilde{N}} \leq R_{\tilde{N}-1} \\ \{\tilde{N} - 1, \tilde{N} - 4, \tilde{N} - 7\}, & \text{otherwise} \end{cases}.$$

Fig. 2.2a summarizes how LLS-CON and its variations select \mathbf{v} on the UAV's trajectory.

2.2.2 LLS-CUM

In LLS-CUM, all the indices of the UAV trajectory are used, rather than a specific number of indices. More specifically, the index set for calculating the location estimate is given by $\mathbf{v} = \{1, \dots, \tilde{N}\}$. The size of the matrices $A_{\mathbf{v}}$ and $b_{\mathbf{v}}$ in (2.8) at index \tilde{N} increases to $(\tilde{N} - 1) \times 3$ and $(\tilde{N} - 1) \times 1$, respectively. The increasing size of the parameter matrices gradually increases the computational complexity as the UAV moves along its trajectory. Fig. 2.2b highlights how LLS-CUM forms the set \mathbf{v} over a UAV's trajectory.

2.2.3 LLS-FML

The main goal of the LLS-FML is to maximize the gap between each index in the set \mathbf{v} . In this algorithm, three indices are used for localization, and the index set is defined as:

$$\mathbf{v} = \left\{ 1, \text{round} \left(\frac{\tilde{N} + 1}{2} \right), \tilde{N} \right\}, \quad \tilde{N} \geq 3.$$

We also study a modified version of LLS-FML, which we refer as LLS-FMLM, which selects the reference locations as

$$\mathbf{v} = \{1, m, \tilde{N}\}, \quad \tilde{N} \geq 3,$$

where the index m is calculated as

$$m = \arg \max_m (d_{1m} + d_{m\tilde{N}}), \quad (2.10)$$

where $d_{1m} = \|(x_1, y_1, z_1) - (x_m, y_m, z_m)\|$ and $d_{m\tilde{N}} = \|(x_{\tilde{N}}, y_{\tilde{N}}, z_{\tilde{N}}) - (x_m, y_m, z_m)\|$. The aim of LLS-FMLM is to maximize the physical total distance separation between the second UAV anchor location and the other two UAV anchor locations. For both LLS-FML and LLS-FMLM, the index array v results in various geometric shapes for the UAV anchor locations, and the localization performance varies based on those geometries. Fig. 2.2c illustrates the operation of LLS-FML and LLS-FMLM.

2.2.4 LLS-CHLM

LLS-CHLM is a geometric approach that exploits the convex hull of the UAV's trajectory. At least three and a maximum of five points of UAV flight are used for generating the set v in this model. When every UAV trajectory is on the same line, a convex is not formed, and for this specific case, the FML algorithm is used. When convex shapes are formed on the UAV's trajectory, a standard algorithm for the convex hull [30] is used to get the boundary location indices that contain all other trajectory points. In this scheme, only the corner points of a convex hull are used to reduce the computational complexity, as shown in Fig. 2.2d.

2.2.5 LLS-CLS

The LLS-CLS takes advantage of the lower path loss at the UAV anchor points that are *closer* to the ground target to be localized. In this model, the three closest indices to the target location are used to form LLS equations. For CLS, the index array v is formed as

$$v = \{v_\phi(1), v_\phi(2), v_\phi(3)\},$$

where v_ϕ is a reordered version of all candidate UAV locations $\{1, \dots, \tilde{N}\}$, sorted by ascending measurement distances to the target node. In other words, LLS-CLS always uses the three

UAV locations that have the closest measurement distance to the target. Note that once the UAV is in the vicinity of the target, the closest three locations are expected to provide a very small localization error. However, it may take a long time for the UAV to fly close to the target depending on the target's location. Moreover, antenna radiation patterns, shadowing, and small-scale fading may negatively affect the accuracy of distance estimates, and hence the accuracy of LLS-CLS, which are not explicitly studied in this chapter. Fig. 2.2e describes the operational principle of LLS-CLS.

2.2.6 Performance Analysis Criteria

Performances of each of the five methods described earlier in this section are evaluated in multiple different ways. First, we evaluate the evolution of the root mean square error (RMSE) of real-time localization as the UAV moves along its trajectory. This provides how fast the localization accuracy gets improved for each approach. Second, we evaluate the RMSE at the endpoint of the UAV trajectory, which we refer to in this study as the *long-term* RMSE, and average the performance over different target locations. We also study the cumulative distribution function (CDF) of the long-term RMSE for all scenarios.

The comparison of the localization performance is based on three criteria. First, localization accuracy is considered, as it is critical for use cases that prioritize high precision over search time. The second criterion is the UAV flight distance as it will directly affect the search time. To measure the flight distance, we define a minimally acceptable localization RMSE threshold (θ) as 20 m. A ground target is assumed to be localized if the localization error is lower than, and does not again become higher than, θ . We define the flight distance when this accuracy is achieved as the required minimum flight distance. The third criterion is reliability. If the RMSE of an algorithm fluctuates as the UAV moves through its trajectory, the algorithm is considered

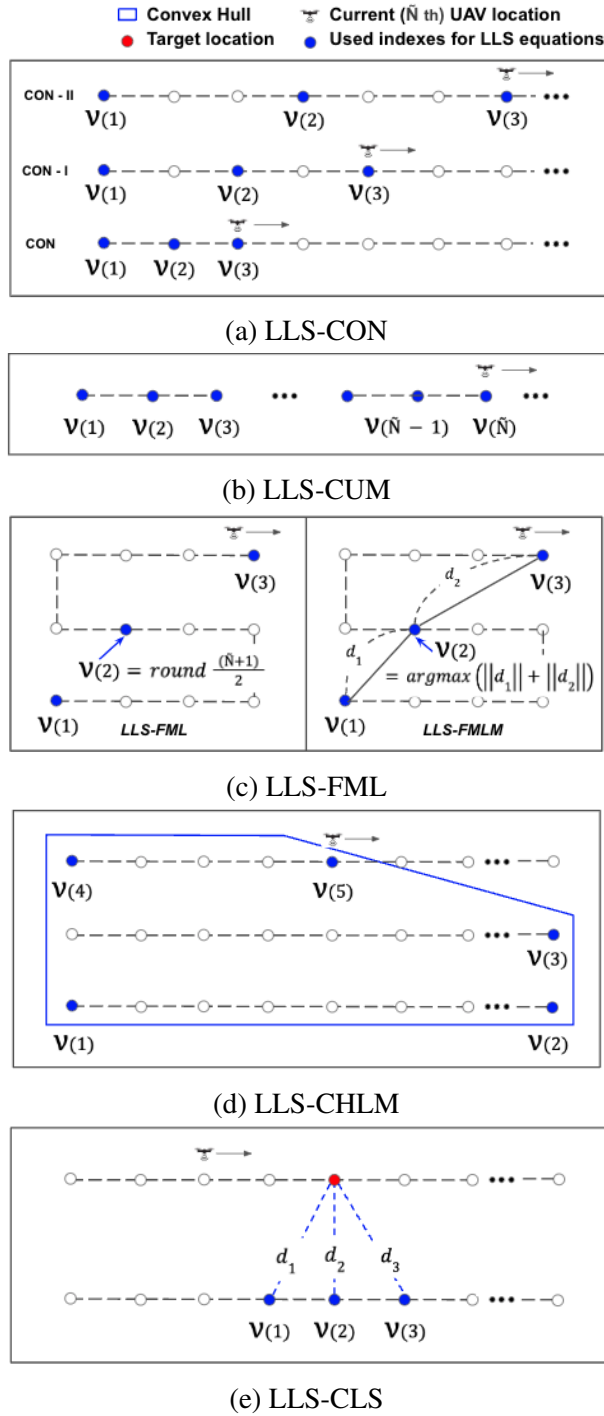


Figure 2.2: Five different SSSL algorithms considered in the free space path loss model.

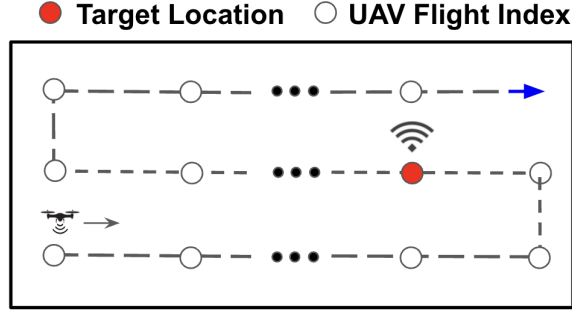


Figure 2.3: Parallel track pattern for SSSL with a UAV.

more unreliable even if it reaches θ early. In this study, the reliability γ is defined as $\gamma = \frac{1}{\sum_{i=2}^N \rho_i}$, where $\rho_i = 1$ if $\text{RMSE}_i \geq \text{RMSE}_{i-1} + \beta$, and $\rho_i = 0$ otherwise, where ρ_i is the mark bit at the i th index of the UAV trajectory, β is the acceptable RMSE gap (assumed to be 1 m in this chapter), and RMSE_i is the RMSE value at the i th index. The reliability of the algorithms can be used as an auxiliary means to select the optimal algorithm in various environments.

2.3 Measurement Results and Analysis

To evaluate the performance of the proposed approaches, a predefined trajectory of a UAV is considered. In particular, we consider the parallel track pattern as shown in Fig. 2.3 which is one of the representative search patterns used when a uniform search is required for a large search area [31, 9]. The UAV flies for 30 m between each waypoint while tracing the 300×300 m open area using the parallel track pattern. There therefore 121 UAV waypoints (indices i) over the UAV's trajectory, each of which forms the candidates for the set \mathcal{v} . The frequency and bandwidth in this study are set to be 2.4 GHz and 20 MHz, respectively [27]. We use two different target location settings. First, the target location is fixed at the center of the map $T(150, 150, 0)$ m, and we compare the performance difference between SRL and DRL for different approaches.

Second, we consider that the target can be located anywhere on a 11×11 grid of resolution on the map, and we average the performance over all the target locations.

2.3.1 Localization Performance for Fixed Target Location

Fig. 2.4 demonstrates the localization performance of SRL and DRL with the five different SSSL algorithms described in Section 2.2, and their variations, when the target location is fixed. The results show that LLS-CON, LLS-CUM, and LLS-CHLM show better localization performance when working with DRL. However, the difference between DRL and SRL is negligible for FML and CLS approaches. Overall, DRL consistently provides better or similar accuracy compared to SRL for reference selection in LLS linearization. Therefore, DRL is employed for the rest of the simulations in this section. The results also show that while the accuracy tends to improve for all scenarios as the UAV moves over its trajectory, for some approaches the accuracy may get worse when v is updated based on new observations.

2.3.2 Average Localization Accuracy

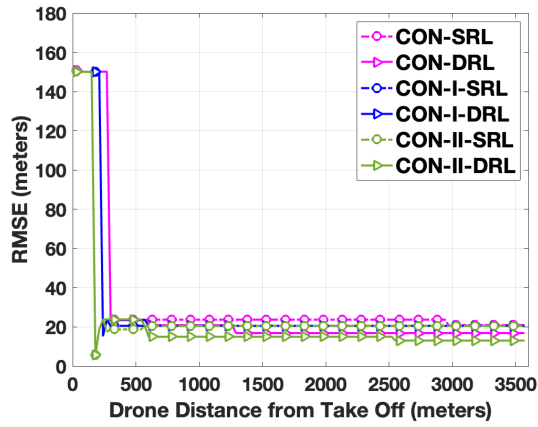
Fig. 2.5 shows the localization performance of each SSSL algorithm based on their RMSE, averaged over the 11×11 ground target grid. We observe that LLS-CON and LLS-CON-I cannot reach the RMSE threshold θ in Fig. 2.5a. LLS-CON-II, LLS-CUM, LLS-FML, and LLS-CHLM show better accuracy with the RMSE range of 12 m to 18 m in Fig. 2.5a, Fig. 2.5b, Fig. 2.5c, and Fig. 2.5d, respectively. In Fig. 2.5e, the LLS-CLS shows the best accuracy as the RMSE converges to 0 at the end. Additionally, Fig. 2.6 shows the performance of each SSSL algorithm based on the CDF of long-term RMSE. Similar to the results of Fig. 2.5, LLS-CLS shows the best performance with the accuracy basis.

When the performance is evaluated based on the UAV flight distance, LLS-CON and LLS-

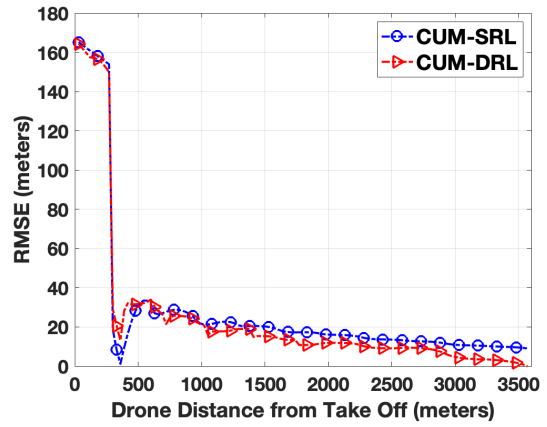
Table 2.2: SSSL algorithms performance summary in the free space path loss model.

Algorithms	$\ v\ $	UAV flight distances (m)	Accuracy (m) (Var (m ²))	Reliability
CON	3	—	21.4659 (31.5793)	1.000
CON-I	3	—	21.5849 (33.1869)	0.500
CON-II	3	2,580	17.965 (33.5379)	0.500
CUM	3 – 5	960	13.115 (13.7559)	0.250
FML	3	2,880	12.283 (14.6101)	0.025
FMLM	3 – 5	—	14.1351 (75.1869)	0.021
CHLM	3 – 5	1,530	14.332 (20.7313)	0.250
CLS	3	3,300	1.067 (0.0843)	0.029

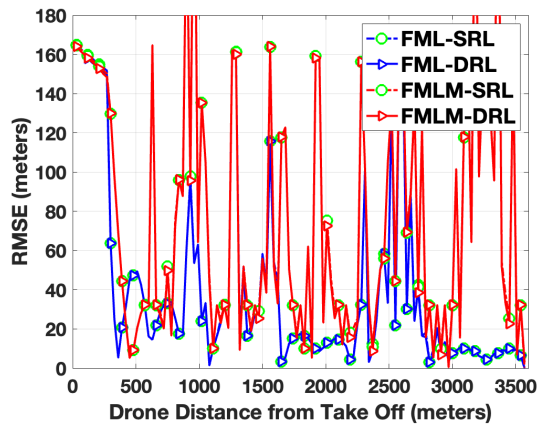
CON-I cannot reach the RMSE threshold θ even with 3,630 m of flight distance which is the maximum flight distance in the given map setting. LLS-CON-II, LLS-FML, and LLS-CLS which show good accuracy require at least 2,580 m, 2,880 m, and 3,300 m of flight distances to reach the desired accuracy. In contrast, LLS-CUM and LLS-CHLM require 960 m and 1,530 m flight distances and are the two quickest SSSL approaches. In terms of reliability, LLS-CON has the best reliability metric. LLS-CUM and LLS-CHLM show relatively better reliability than LLS-FML and LLS-CLS. In Table. 2.2, we summarize the performances of all the SSSL approaches considering different evaluation criteria.



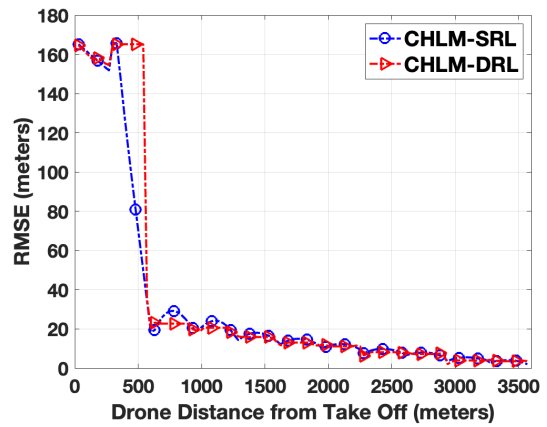
(a) LLS-CON, LLS-CON-I, LLS-CON-II



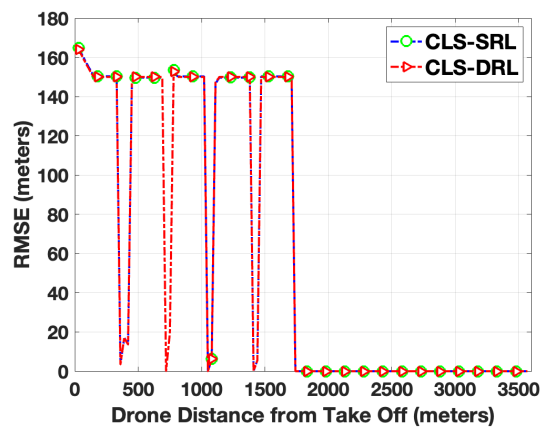
(b) LLS-CUM



(c) LLS-FML and LLS-FMLM

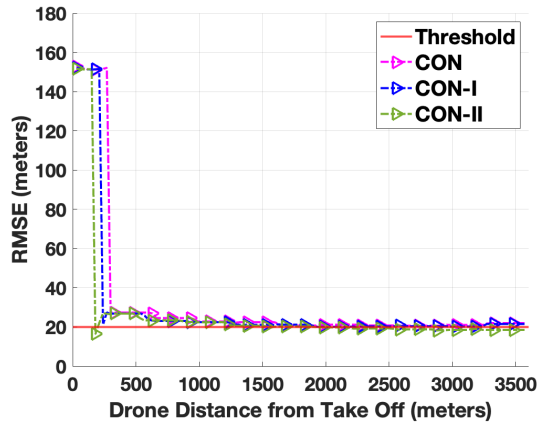


(d) LLS-CHLM

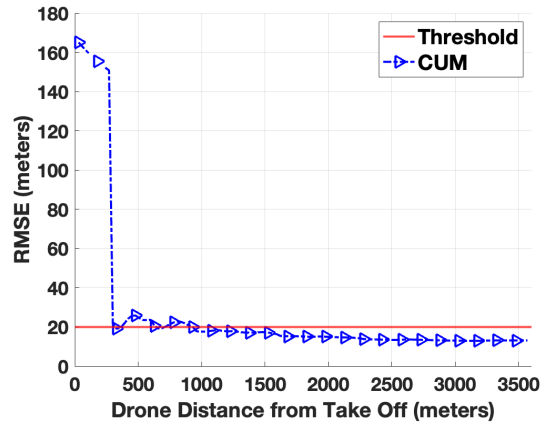


(e) LLS-CLS

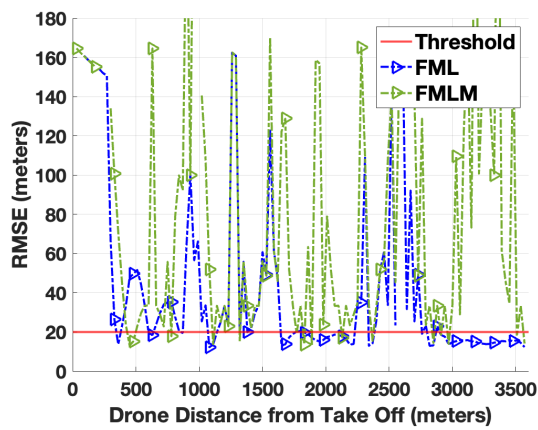
Figure 2.4: Comparison of SRL and DRL for a fixed target location considering five different SSSL approaches and their variations in the free space path loss model.



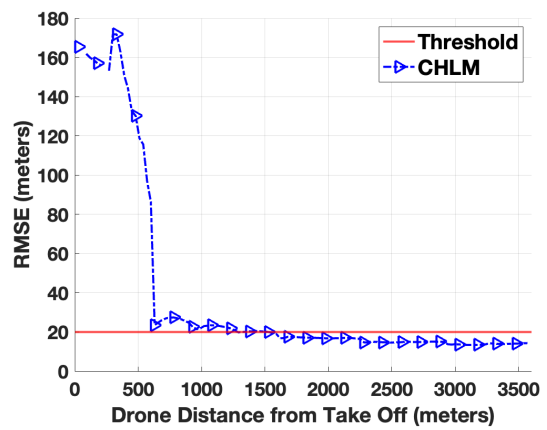
(a) LLS-CON, LLS-CON-I, LLS-CON-II



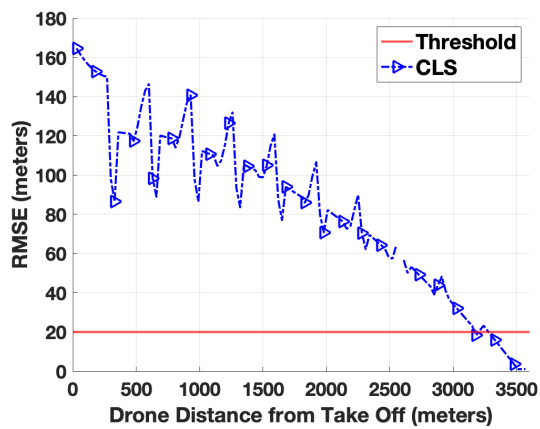
(b) LLS-CUM



(c) LLS-FML and LLS-FMLM



(d) LLS-CHLM



(e) LLS-CLS

Figure 2.5: RMSE of five different SSSL approaches and their variations averaged over different target locations in the free space path loss model.

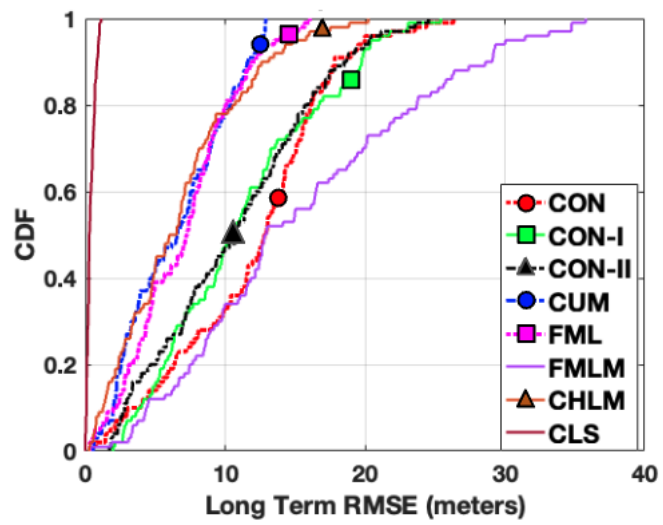


Figure 2.6: CDF of RMSE averaged over different target locations in the free space path loss model.

CHAPTER

3

RF SSSL BY AN AUTONOMOUS UAV WITH TWO-RAY CHANNEL MODEL AND DIPOLE ANTENNA PATTERNS

3.1 System Model

The coordinates of a transmitter that is to be localized are represented as $l^T = (x, y, z)$. The receiver's (UAV's) location at the i_{th} discretized coordinate is expressed as $l^D = (x_i, y_i, z_i)$. We assume that the UAV altitude is fixed for a given SSSL mission, hence, $z_i = h$. Considering a

two-ray propagation model, the received signal strength can be characterized as follows [32]:

$$P_r = P_t \left(\frac{\lambda}{4\pi} \right)^2 \left| \frac{\sqrt{G(\theta_l)}}{d_{\text{los}}} + \Gamma(\theta_r) \sqrt{G(\theta_r)} \frac{e^{-j\Delta\phi}}{d_{\text{ref}}} \right|^2, \quad (3.1)$$

where P_r is received signal strength, P_t is transmitted signal strength, λ is $\frac{c}{f}$, $\theta_l = \tan^{-1}(\frac{z-h}{d_{2D}})$ is the elevation angle between the transmitter and the receiver and $\theta_r = \tan^{-1}(\frac{z+h}{d_{2D}})$ is the ground reflection angle. To calculate θ_l and θ_r , we use $d_{2D} = \sqrt{(x-x_i)^2 + (y-y_i)^2}$. Moreover, $G(\theta_l)$ is the antenna gain of the line of sight and $G(\theta_r)$ is the antenna gain of the ground reflected ray. In this context, the antennas of both the transmitter and the receiver are oriented vertically. Based on these assumptions, the antenna gains can be represented as a function of the spatial coordinates pertaining to the transmitter and the receiver in the following manner [33]:

$$G(\theta) = G(l^T, l^D) = \frac{\cos(\frac{\pi l f}{c} \sin(\theta)) - \cos(\frac{\pi l f}{c})}{\cos(\theta)}, \quad (3.2)$$

where $l = \frac{\lambda}{2}$ is the wavelength that is assumed to be a half-wave dipole antenna in this chapter. In (3.1), $\Gamma(\theta)$ is the ground reflection coefficient and it is represented as [34]

$$\Gamma(\theta_r) = \frac{\sin(\theta_r) - \sqrt{\epsilon_0 - \cos^2(\theta_r)}}{\sin(\theta_r) + \sqrt{\epsilon_0 - \cos^2(\theta_r)}}, \quad (3.3)$$

where $\epsilon_0 = \epsilon - j60\Psi\lambda$ is an environment constant that represents the relative permittivity of the ground. This value depends on the two components of ground type: i) Ψ represents the conductivity of the earth (units in mhos per meter), and ii) ϵ denotes the dielectric constant of the ground relative to unity in free space.

In (3.1), $\Delta\phi$ is the phase difference between the line of sight and the reflected paths by the

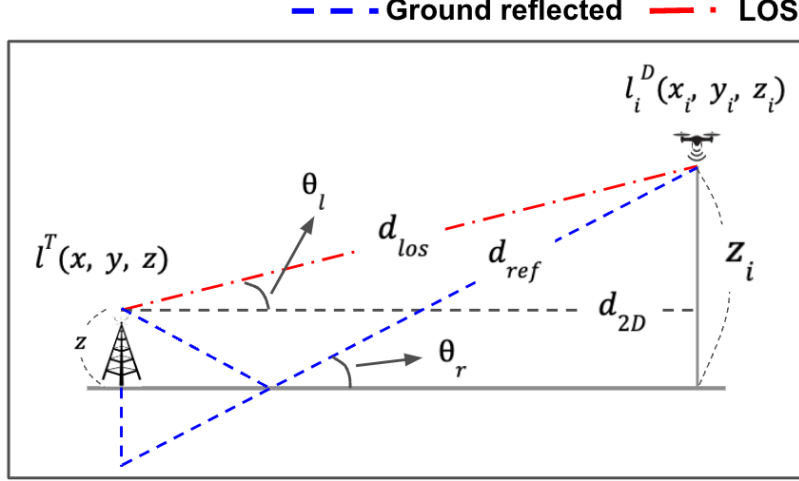


Figure 3.1: Two-ray propagation model.

different arrival time, which can be expressed as

$$\Delta\varnothing = \frac{2\pi(d_{\text{ref}} - d_{\text{los}})}{\lambda}, \quad (3.4)$$

where d_{los} and d_{ref} are the line of sight distance between the transmitter and the i_{th} receiver and the reflected distance from each, respectively. They can be expressed as functions of l^T and l^D as follows

$$d_{\text{los}_i}(l^T, l^D) = \sqrt{(x - x_i)^2 + (y - y_i)^2 + (z - h)^2}, \quad (3.5)$$

$$d_{\text{ref}_i}(l^T, l^D) = \sqrt{(x - x_i)^2 + (y - y_i)^2 + (z + h)^2}. \quad (3.6)$$

We assume that the transmitted signal strength of the target is known by the UAV. Then, the path loss at each receiver's location can be modeled by

$$\text{PL}_i = P_t - P_{r_i} + \omega_i, \quad (3.7)$$

where ω denotes shadowing component that follows a zero-mean Gaussian distribution $\omega \sim N(0, \sigma^2)$. Then, the measured path loss by the received signal strength at the i_{th} location can be expressed as

$$\widetilde{\text{PL}}_i = P_t - P_{r_i} . \quad (3.8)$$

To implement the least square algorithm for localization, the distance between the target and the i_{th} receiver's locations needs to be estimated. We assume that the two-dimensional separation between the transmitter and the receiver can be estimated based on the residuals between the measured path loss and the path loss by the analytical model. The estimated distance based on the difference in path loss can be formulated as follows

$$\hat{d}_{2\text{D}} = \arg \min_d \left(\widehat{\text{PL}}_i - \widetilde{\text{PL}}_i \right)^2 , \quad (3.9)$$

where $\hat{d}_{2\text{D}}$ represent the estimated distance between the target and the i_{th} UAV location in two dimensions, $\widetilde{\text{PL}}_i$ denote the measured path loss, and $\widehat{\text{PL}}_i$ indicates the analytically derived path loss using (3.1). Note that $\widehat{\text{PL}}_i$ is a function of a single variable $d_{2\text{D}}$ since the parameters of this equation, $G(\theta)$, $\Gamma(\theta r)$, d_{los} , and d_{ref} , can be expressed in terms of $d_{2\text{D}}$.

Assuming that the index of the current location of the UAV is denoted as \tilde{N} , we only utilize the subset of indices to estimate the target location. The size of the selected unique indices to be used in the localization process should be $3 \leq S \leq \tilde{N}$. The subset of indices can be represented as \mathcal{v} . In addition, a reference index r_{th} , $r \in \mathcal{v}$, is defined for each suggested localization algorithm, which is used to obtain $|S - 1|$ linear equations from S expressions. In this chapter, the closest index among the indices \mathcal{v} from the target is set as a reference index. Once the estimated distance has been determined, the transmitter's position can be approximated by employing the

least square approach for $k = 1, \dots, S$, and $k \neq r$, as [35]

$$A_v l_{2D}^T = b_v, \quad (3.10)$$

where

$$A_v = 2 \begin{bmatrix} x_{v(1)} - x_r & y_{v(1)} - y_r \\ \vdots & \vdots \\ x_{v(k)} - x_r & y_{v(k)} - y_r \\ \vdots & \vdots \\ x_{v(S)} - x_r & y_{v(S)} - y_r \end{bmatrix}, \quad (3.11)$$

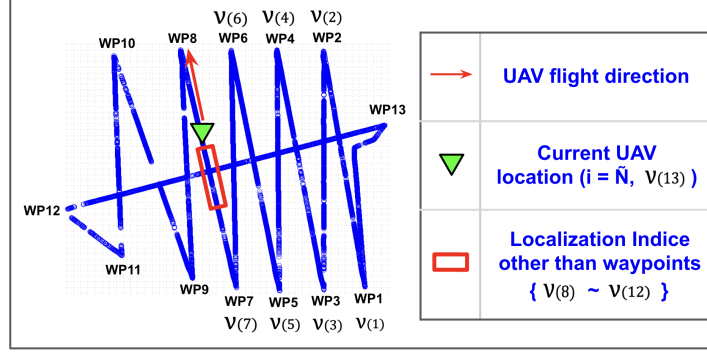
$$b_v = \begin{bmatrix} d_r^2 - d_{v(1)}^2 + x_{v(1)}^2 + y_{v(1)}^2 - \chi \\ \vdots \\ d_r^2 - d_{v(k)}^2 + x_{v(k)}^2 + y_{v(k)}^2 - \chi \\ \vdots \\ d_r^2 - d_{v(S)}^2 + x_{v(S)}^2 + y_{v(S)}^2 - \chi \end{bmatrix}, \quad (3.12)$$

and $l_{2D}^T = [\hat{x}, \hat{y}]^T$ is the estimated target location, where $v(k)$ is k_{th} index of v , $d_{v(k)}$ is estimated distance between the target and the receiver gained based on (3.9), and χ is $(x_r^2 + y_r^2)$. The estimated target location l_{2D}^T can then be determined employing the least square solution, given by

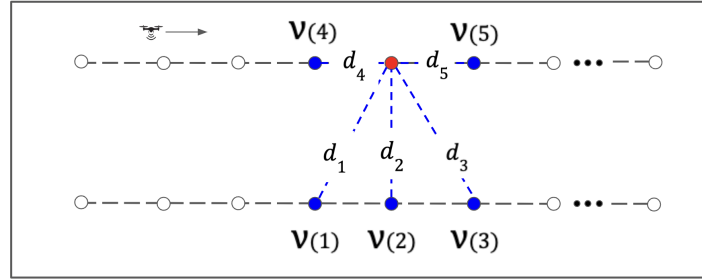
$$l_{2D}^T = (A_v^T A_v)^{-1} A_v^T b_v. \quad (3.13)$$



(a) LLS-CUM



(b) LLS-CHLM



(c) LLS-CLS

Figure 3.2: SSSL algorithms considered in the two-ray propagation model.

3.2 Proposed SSSL Methods

In the previous chapter, five heuristic-based localization algorithms were proposed for the selection of indices v on the UAV's trajectory for constructing equations as indicated in (3.13):

- 1) LLS-CON: utilizing three consecutive indices from the current UAV's flight index \tilde{N} , given by $v = \{\tilde{N}, \tilde{N} - 1, \tilde{N} - 2\}$;
- 2) LLS-CUM: using every index up to the current UAV's flight index \tilde{N} , denoted as $v = \{1, \dots, \tilde{N}\}$;
- 3) LLS-FML: selecting the first, middle, and last index, which can be expressed as $v = \left\{1, \text{round}\left(\frac{\tilde{N}+1}{2}\right), \tilde{N}\right\}$;
- 4) LLS-CHLM: adopting three to five indices

using the concept of the convex hull in which the connected lines of each index encompass all other indices of the UAV's trajectory; and 5) LLS-CLS: selecting three indices that are the closest to a target location, which can be represented as $v = \{v_\phi(1), v_\phi(2), v_\phi(3)\}$, where v_ϕ is a reordered by ascending manner.

In previous work, these algorithms were evaluated in a simplified simulation scenario, utilizing the free space path loss model and minimizing noise factors to reduce the inherent randomness of the simulations. On the other hand, the present study aims to investigate the performance of these localization algorithms in more realistic environments, considering the two-ray propagation model in an open field and using more realistic antenna patterns. In the current simulation setup, the interval between each index on the UAV's trajectory, where RF measurements from the target are taken, is much shorter than what is used in [35]. Hence, we decided not to implement LLS-CON. In addition, given its poor localization accuracy in [35], LLS-FML is also not included in this study. In the end, the LLS-CUM, LLS-CHLM, and LLS-CLS are used and compared with each other in this chapter.

In the current research, the number of indices on the UAV's trajectory is updated as follows for different SSSL approaches to accommodate the new simulation environment.

LLS-CUM

The same index array as the previous study is used as $v = \{1, \dots, \tilde{N}\}$.

LLS-CHLM

A total of thirteen indices are used based on the number of predefined trajectory's waypoints (WPs). In this modified algorithm, consecutive thirteen indices are used before the UAV reaches the WPs. However, as the UAV passes each WP, index array v is updated in a way to have a WP

passing index as a member. The index array for the LLS-CHLM is denoted as

$$\mathbf{v} = \{\tilde{N}, \tilde{N} - 1, \dots, \tilde{N} - (12 - j), \dots, \text{WP}_1, \dots, \text{WP}_j\},$$

$$\tilde{N} \geq 13, \text{ and } 2 \leq j \leq 13,$$

where WP_j is the j_{th} WP upon the preplanned trajectory.

LLS-CLS

Uses five trajectory indices for better performance. As the interval of each index becomes narrowed, the consecutive three points tend to have limited localization performance. As we assume that \mathbf{v}_ϕ is a reordered array of \mathbf{v} in an ascending manner, the index array used for implementation of the LLS-CLS is represented as

$$\mathbf{v} = \{v_\phi(1), v_\phi(2), v_\phi(3), v_\phi(4), v_\phi(5)\}.$$

Figure 3.2 presents the underlying frameworks of each localization algorithm being considered in this study.

3.3 Measurement Results and Analysis

The experiments are carried out in MATLAB-based simulations. During the simulation stage, the theoretical received signal strength (RSS) is evaluated based on the two-ray propagation model. The three proposed localization algorithms are then implemented and comparatively assessed in terms of their localization performance. In this stage, the transmitter's and receiver's antenna patterns are set to two separate configurations: 1) omnidirectional antenna pattern; and 2) doughnut-shaped dipole antenna pattern. Finally, to evaluate localization algorithm performance,

Table 3.1: Summary of simulation parameters in the two-ray propagation model.

Channel model	
Carrier frequency	2.4 GHz
Bandwidth	20 MHz
Path loss exponent	2
Transmitter	
Height	1 m
Transmit power	76 dBm
Antenna gain (Omni)	2 dBi
UAV	
Altitude	{30, 50, 70} m
Antenna gain (Omni)	2 dBi

three components were implemented consistent with the previous study: 1) accuracy; 2) time used to achieve a specific level of localization accuracy; and 3) reliability.

In simulations, the frequency and bandwidth for the transmitted signal are set as 2.4 GHz and 20 MHz, respectively. We employed a zig-zag pattern for the UAV's trajectory. In addition, the transmitter is positioned in three different locations: 1) the target is on the UAV's predefined trajectory; 2) the target is at the boundary of the trajectory; and 3) the target is in a position far away from the trajectory. This approach enabled the analysis of localization performance based on the distance of the signal source from the predefined trajectory. The trajectory and the different target locations are represented in Fig. 3.3. For the antenna pattern configuration, the omnidirectional antenna pattern's gain is set to 2 dBi for simplicity. On the other hand, the doughnut-shaped dipole antenna gain is set based on (3.2). The principal distinction between the dipole antenna and the omnidirectional antenna pattern lies in the variation of antenna gain as the UAV's altitude changes.

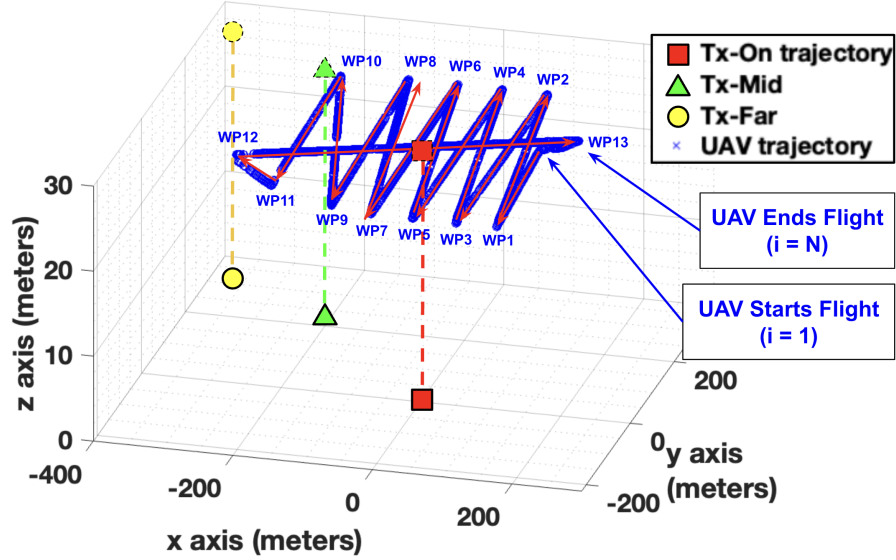


Figure 3.3: Trajectory of the UAV with fixed waypoints, and three different signal source locations that the UAV is searching in the two-ray propagation model. While all the target locations are on the ground, their corresponding locations at the UAV’s altitude are also illustrated, to show their relative location with respect to the UAV’s trajectory more clearly.

3.3.1 Analysis of RSS for Different Scenarios

Using the simulation assumptions described earlier, the RSS observations at different UAV altitudes, which are to be used for different SSSL algorithms, are summarized in Figs. 3.4-3.5. The theoretical RSS is obtained based on (3.7), while the measured RSS is also derived from the same equation but includes a Gaussian noise component. Fig. 3.4 depicts the variation of RSS as a function of the distance between the transmitter and the receiver. Fig. 3.5 represents RSS in relation to the UAV’s trajectory. In these figures, RSS at close distances to the target location is significantly influenced by the UAV’s altitude. Using these measurements, the proposed localization algorithms are executed and compared across different UAV altitudes in the following section.

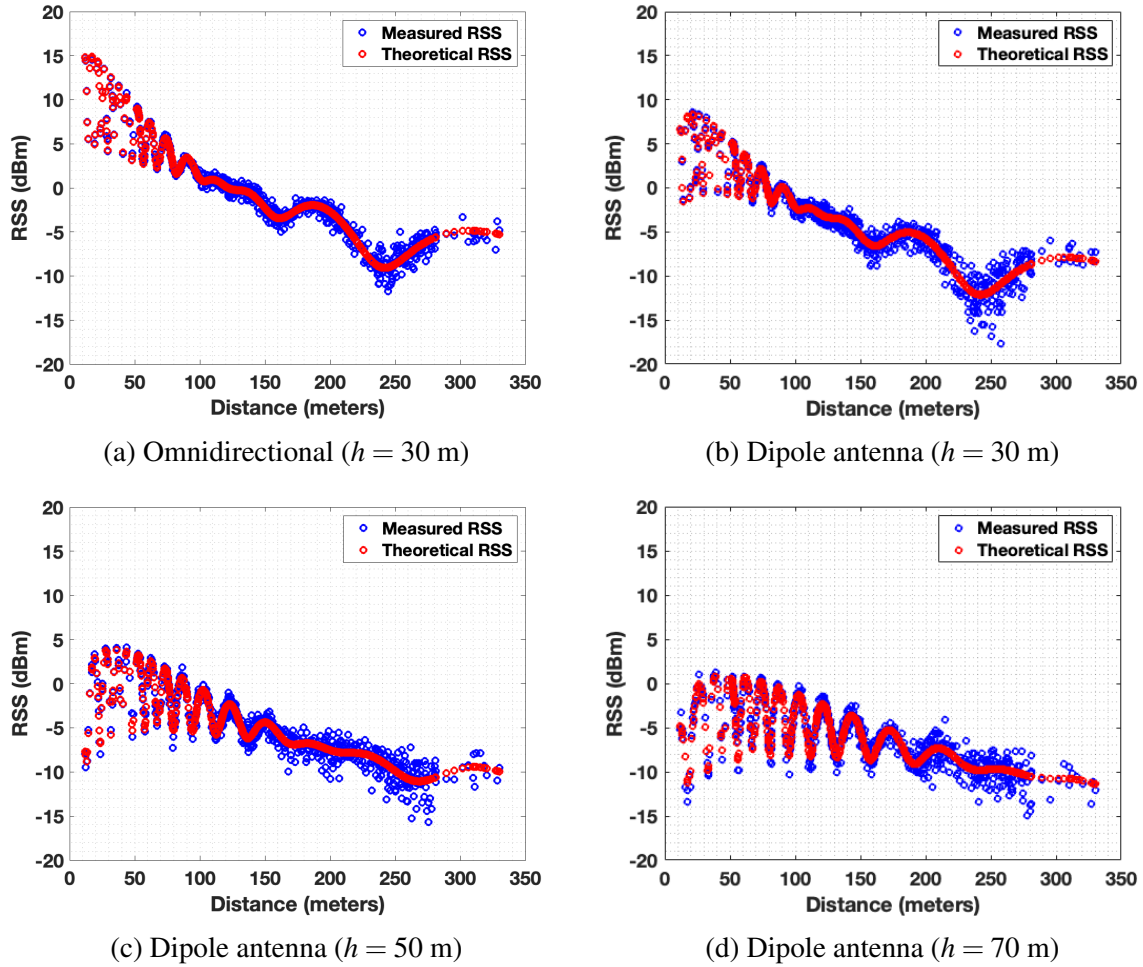


Figure 3.4: RSS measurements for various scenarios in the two-ray propagation model: RSS vs. distance.

3.3.2 Analysis of Distance Estimation Accuracy

In this section, we analyze how the accuracy of distance and location estimates change with respect to the true distance and angle between the UAV and the ground target. The root mean square error (RMSE) of the distance estimates using (3.9) as a function of the distance (DROD) and angle (DROA) between the UAV and the ground target are depicted in Figs. 3.6-3.7. In addition, the RMSE of the location estimates using (3.13) as a function of the distance (LROD)

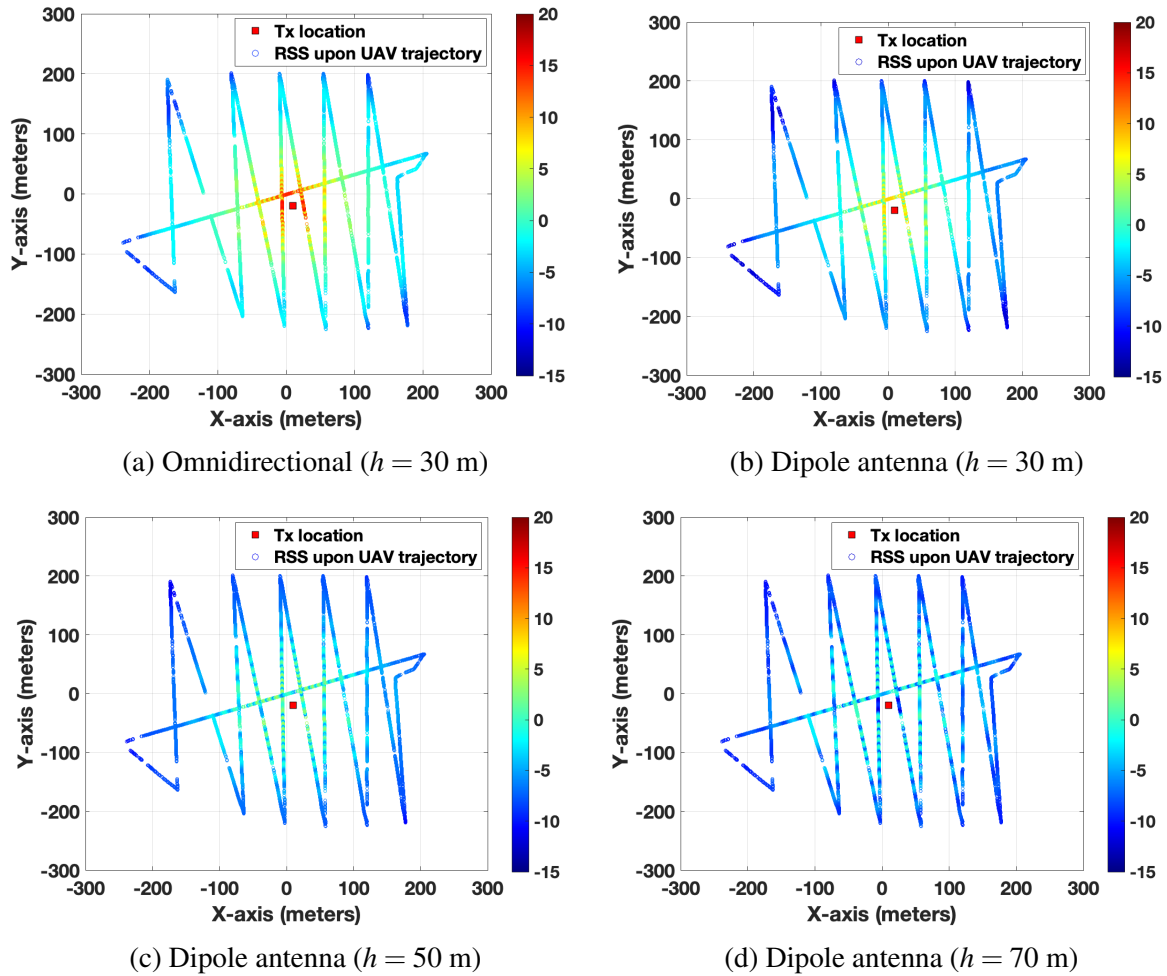


Figure 3.5: RSS measurements for various scenarios in the two-ray propagation model: RSS vs. trajectory.

and angle (LROA) between the UAV and the ground target are illustrated in Figs. 3.8-3.9. The RMSE of the estimated distance has proportional relations with the real distance for both omnidirectional and dipole antenna patterns when the altitude of the UAV is below 50 meters. On the other hand, when the UAV is at an altitude of 70 meters, the close distances also result in poor estimation due to weaker signal strength caused by the dipole antenna pattern. Similar trends in the relationship between distance estimation RMSE and angle are also shown. Assuming that

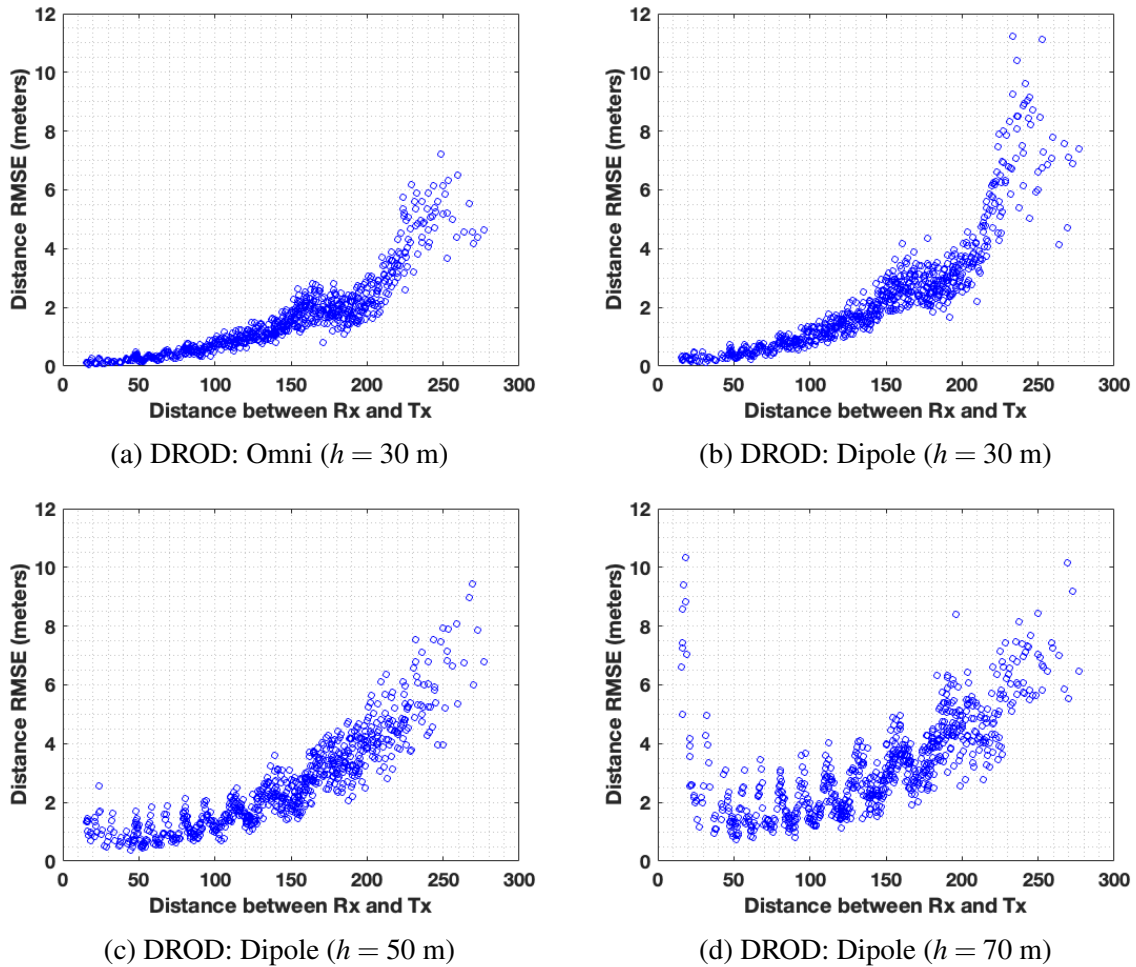


Figure 3.6: Distance estimation RMSE for distance variation in the two-ray propagation model.

the altitude of the UAV is fixed in each experiment, the angle variation is mainly affected by the distance. In the figures, larger angles exhibit lower RMSE on distance estimates for both antenna patterns when the UAV altitude is below 50 meters. However, the distance estimation RMSE increases at higher angles when the UAV is at an altitude of 70 meters.

The impact of angle and distance variations on localization performance is also illustrated in Figs. 3.8-3.9. The angle and distance differ at every trajectory index, so tracking the characteristics of each index is crucial. From this perspective, the LLS-CHLM algorithm is implemented

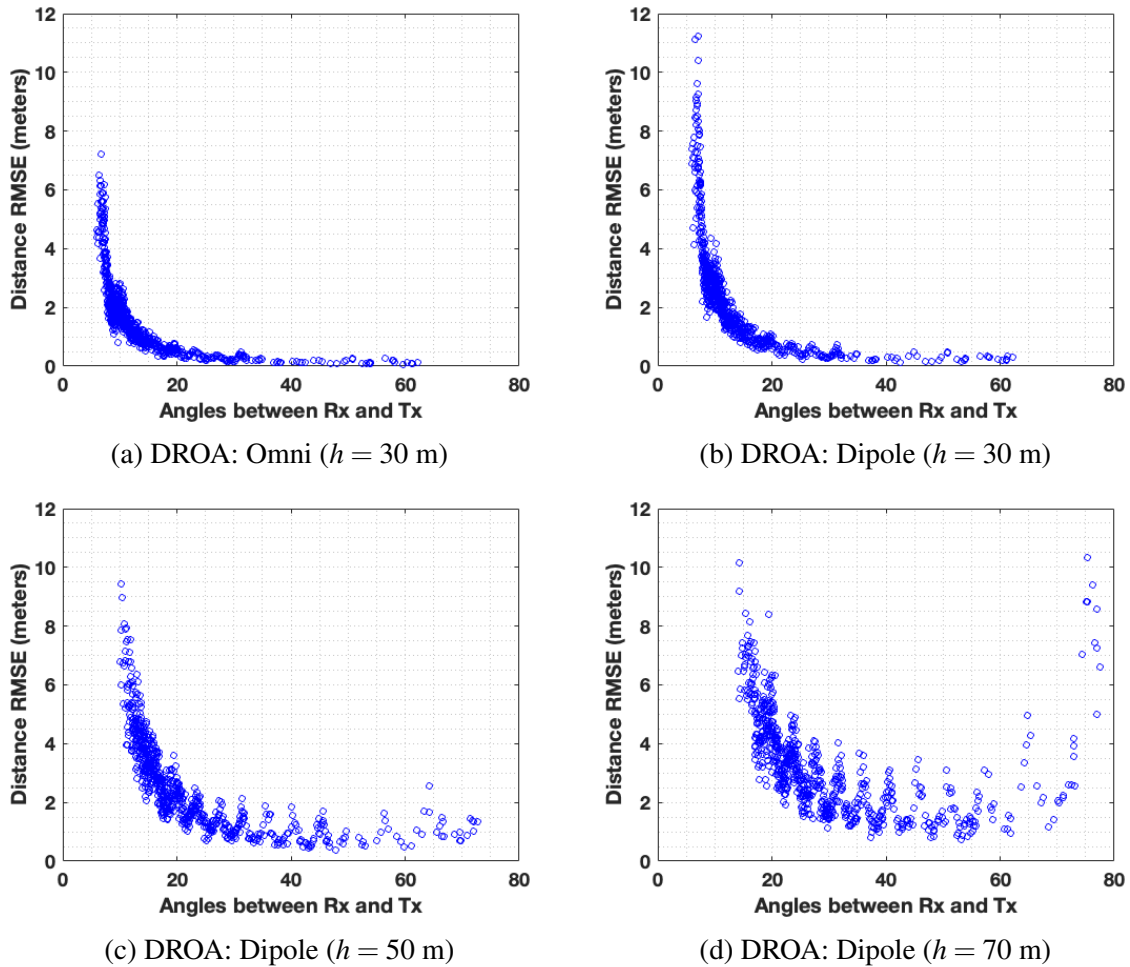


Figure 3.7: Distance estimation RMSE for angle variation in the two-ray propagation model.

for localization results in Figs. 3.8-3.9. Recalling the features of the other two algorithms: 1) the LLS-CLS only uses the closest five indices, and 2) the LLS-CUM uses every index up to the current flight index, they cannot explicitly represent the influence of each index. In addition, to clearly observe the variation in distance and angle, the transmitter is positioned at the center of the UAV's trajectory. In Fig. 3.8, it is observed in all antenna patterns and UAV altitudes that larger distances cause higher localization RMSE. On the other hand, higher angles result in a lower localization RMSE. One remarkable observation is the discrepancy in how the distance

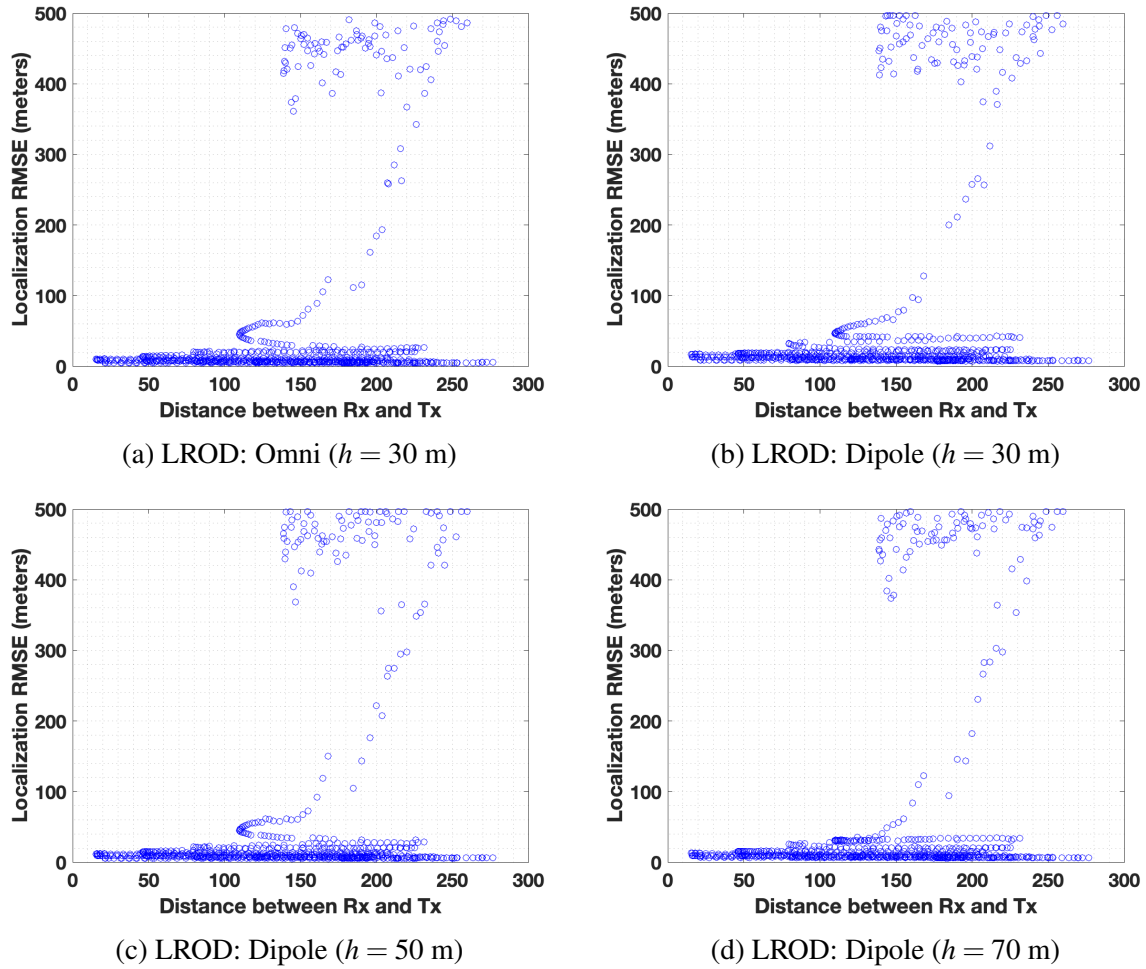


Figure 3.8: Location estimation RMSE for distance variation in the two-ray propagation model.

and localization errors depend on angle when the UAV altitude is at 70 meters. In Fig. 3.7d, the distance RMSE increased when the angle is larger than 60 degrees. On the other hand, in Fig. 3.9d, the localization RMSE is stabilized after 30 degrees. In this case, the possible localization error caused by the distance error is mitigated by other indices when using the least-square localization algorithm.

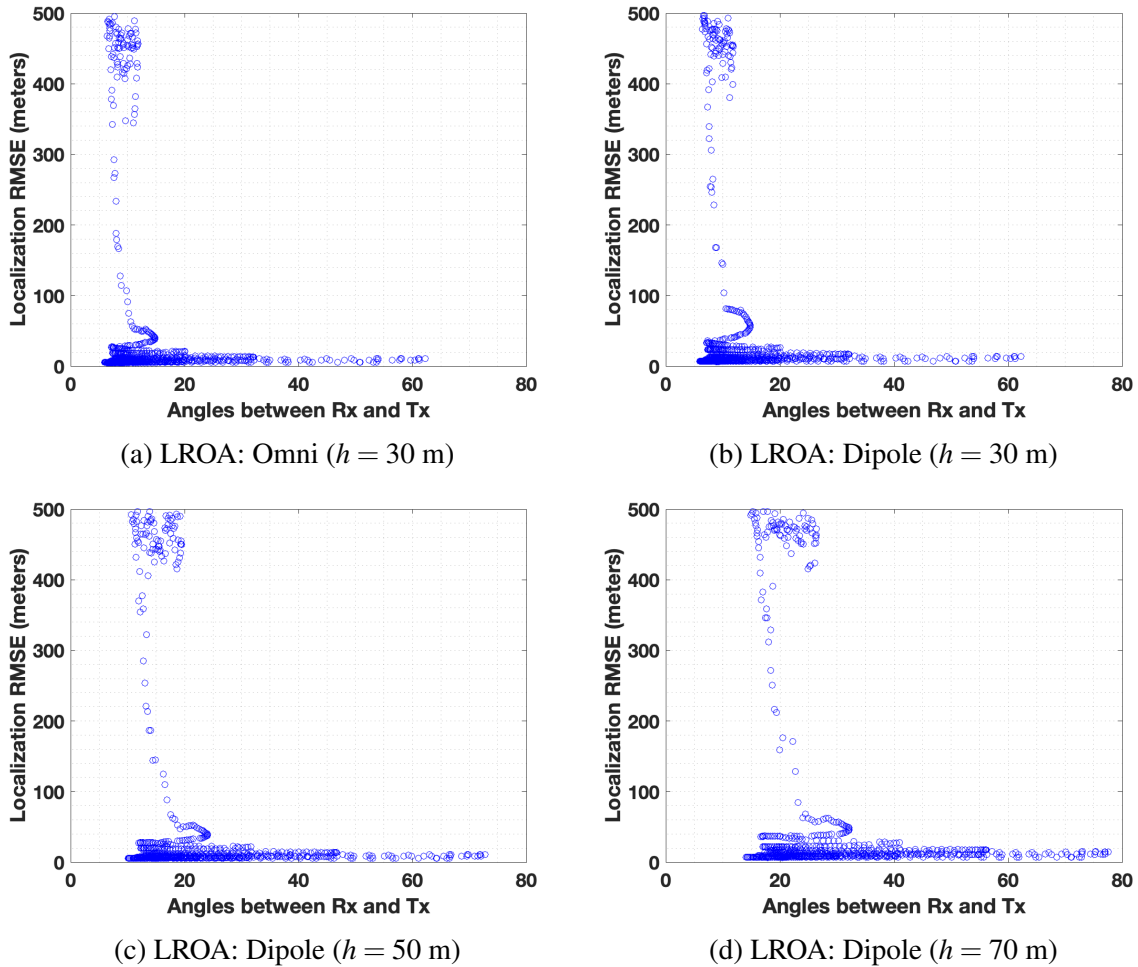


Figure 3.9: Location estimation RMSE for angle variation in the two-ray propagation model.

3.3.3 Analysis of Proposed SSSL Methods

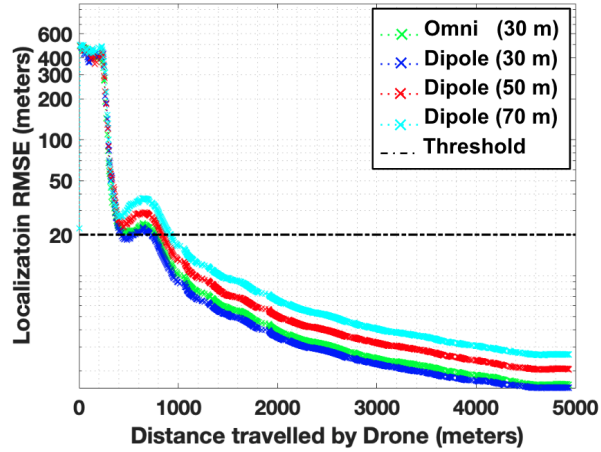
Utilizing the estimated distances and least-square approach, we implemented and compared the proposed localization algorithms for the omnidirectional antenna pattern at a UAV altitude of 30 meters and the dipole antenna pattern at UAV altitudes of 30, 50, and 70 meters, as depicted in Figs. 3.10-3.12. In this figure, the x-axis represents the distance traveled by the UAV, while the y-axis indicates the localization RMSE. For performance comparison, we set a localization RMSE threshold at 20 meters. For on-target location setup, the LLS-CUM achieves

the localization RMSE threshold in the shortest flight time. However, for mid-target and far-target setups, the LLS-CHLM and LLS-CUM exhibit similar localization performance for both dipole and omnidirectional antenna configurations, while the LLS-CLS demonstrates unreliable performance, particularly in far-target settings.

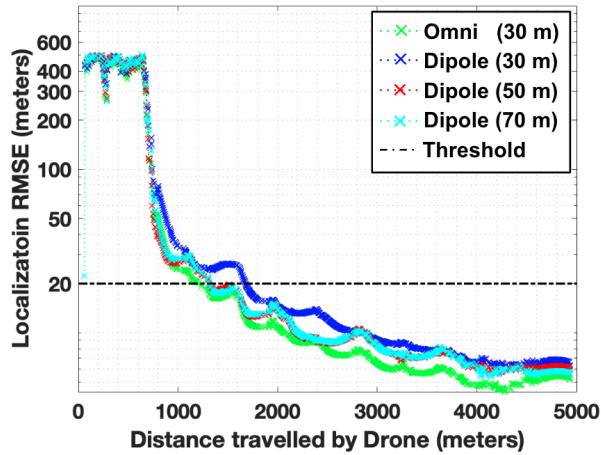
Fig. 3.13 presents the long-term localization RMSE for each algorithm with respect to target variation and the required flight time to reach the RMSE threshold in the CDF graphs. For simplicity and to distinguish the antenna pattern's impact, we primarily consider the dipole antenna pattern with a UAV altitude of 50 meters. The LLS-CLS delivers the best localization accuracy in on-target (1.8814 meters) and mid-target (2.6457 meters) scenarios. However, the same algorithm exhibits the worst performance for the far-target scenario, as the UAV's trajectory does not pass nearby the target. Both the LLS-CUM and LLS-CHLM demonstrate relatively similar localization accuracy in every target setup. For the required flight time measurement, we assume a maximum UAV flight speed of 20 m/s and an acceleration speed of 5 m/s^2 . The required flight time for LLS-CLS is heavily influenced by the target's position, with the current target configuration showing the longest flight time for the required localization accuracy. The other two algorithms display similar performance in terms of required time, with LLS-CUM requiring slightly less flight time than LLS-CHLM in the overall target configurations. Table 3.2 summarizes the performances of all SSSL approaches, considering different evaluation criteria.

Table 3.2: SSSL algorithms performance summary in the two-ray propagation model.

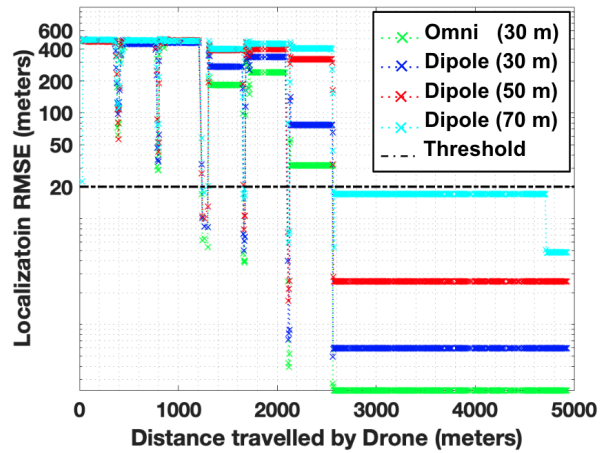
Algorithms	UAV flight time (seconds)	UAV flight distances (m)	Average long term accuracy (m) (Var (m²))
CUM-On	35.9	683.6	2.0058 (1.5653)
CHLM-On	77.3	1,369.1	5.8384 (19.5932)
CLS-On	142.9	2,462.6	1.8814 (1.6371)
CUM-Mid	156.6	2,782.5	11.2024 (77.2772)
CHLM-Mid	125.8	2,192.2	7.7171 (20.4467)
CLS-Mid	238.6	4,142.6	2.6457 (3.0880)
CUM-Far	240.4	4,190.5	14.2262 (124.4173)
CHLM-Far	244.6	4,225.9	15.6131 (100.1289)
CLS-Far	—	—	85.8901 (2,883.2)



(a) On target: LLS-CUM

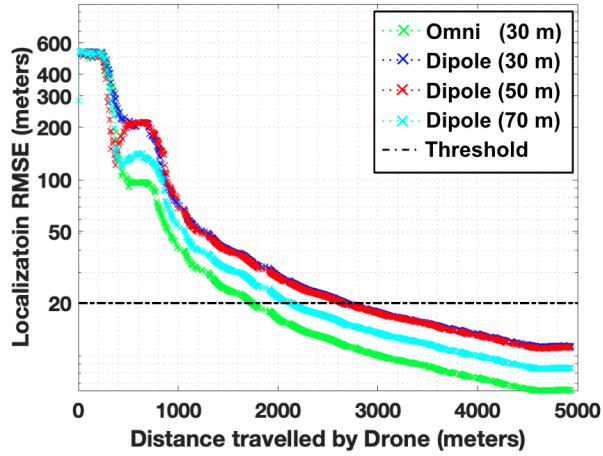


(b) On target: LLS-CHLM

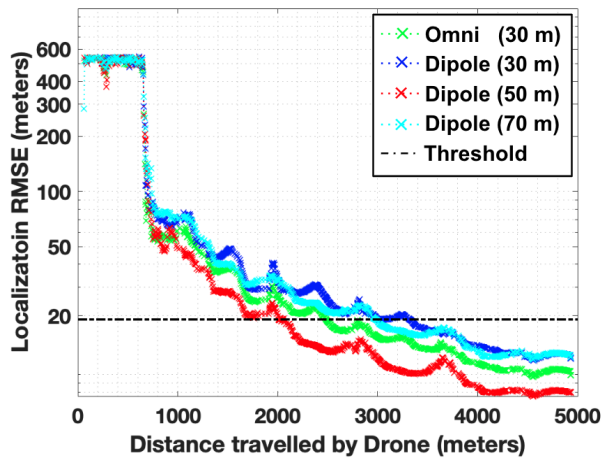


(c) On target: LLS-CLS

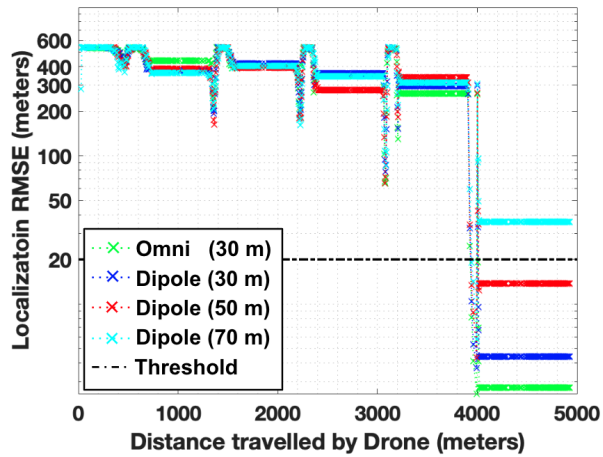
Figure 3.10: Localization RMSE comparison upon on-target locations in the two-ray propagation model: Omni, Dipole (with altitude 30m, 50m, and 70m)



(a) Mid target: LLS-CUM

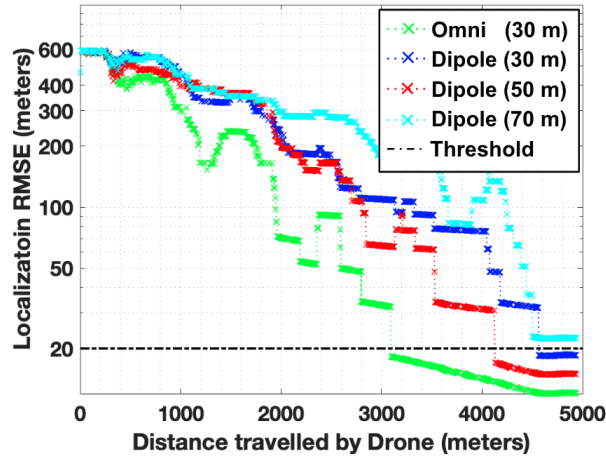


(b) Mid target: LLS-CHLM

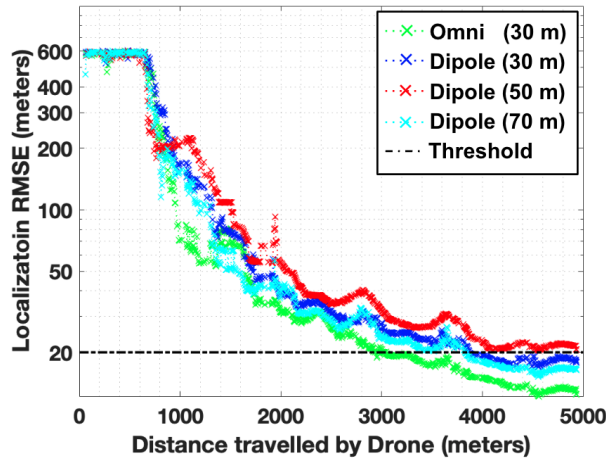


(c) Mid target: LLS-CLS

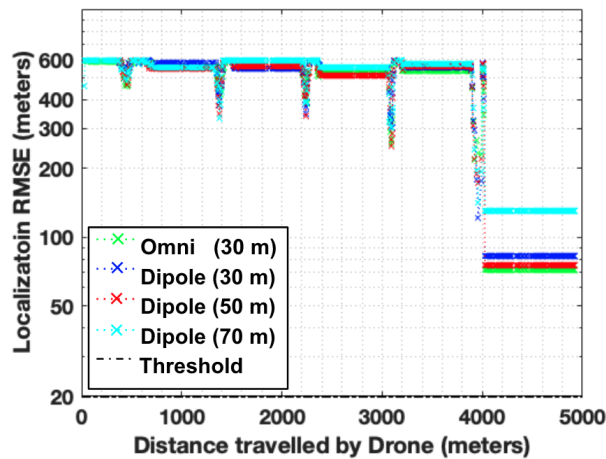
Figure 3.11: Localization RMSE comparison upon mid-target locations in the two-ray propagation model: Omni, Dipole (with altitude 30m, 50m, and 70m)



(a) Far target: LLS-CUM

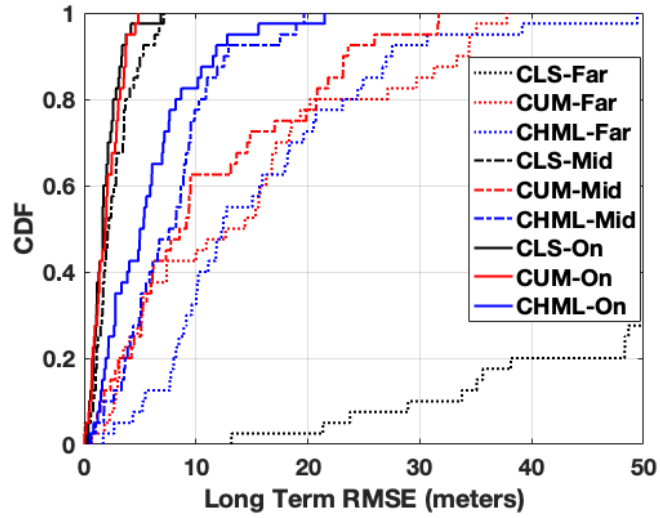


(b) Far target: LLS-CHLM

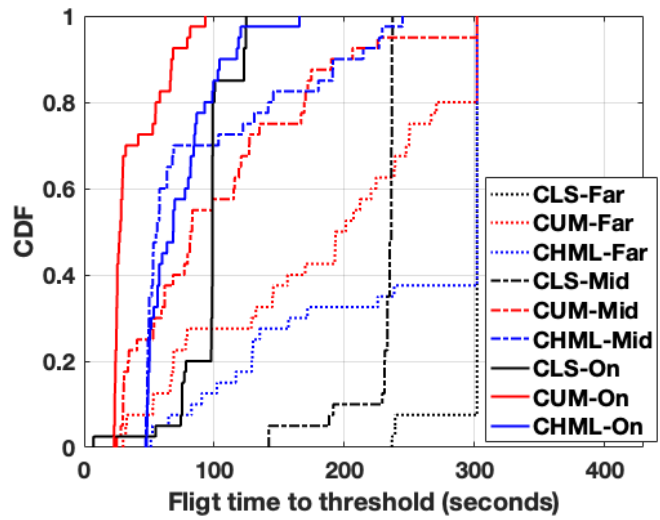


(c) Far target: LLS-CLS

Figure 3.12: Localization RMSE comparison upon far-target locations in the two-ray propagation model: Omni, Dipole (with altitude 30m, 50m, and 70m)



(a) Long term RMSE CDF



(b) Flight time CDF

Figure 3.13: CDFs of the localization error and localization time for different techniques and scenarios in the two-ray propagation model.

CHAPTER

4

CONCLUSIONS AND FUTURE WORK

In Chapter 2, we investigate the SSSL problem by considering five different approaches for selecting anchor locations on a UAV's trajectory. Using computer simulations, we show that LLS-CLS shows the best performance in terms of localization accuracy. However, it requires a relatively long flight distance, and hence, a longer search time. On the other hand, LLS-CUM has the best performance based on the flight distance. However, it requires high computational complexity due to the increasing size of parameter matrices that are used for finding the location estimate. With this analysis, the LLS-CHLM shows to have a fairly good performance trade-off for accuracy, flight distance, and reliability, and it requires a low computational complexity.

In Chapter 3, we study the SSSL problem with an autonomous UAV, considering three

distinct approaches for selecting anchor locations along a UAV's trajectory. We incorporate a two-ray propagation model and specific UAV antenna patterns into our simulation setup. We demonstrate that the LLS-CLS algorithm excels in terms of localization accuracy when the target is in close proximity to the UAV's trajectory. However, it falls short of achieving the required localization accuracy when the target is far from the trajectory. In contrast, the other two algorithms, LLS-CUM and LLS-CHLM, display similar and relatively stable localization performance in terms of both accuracy and required search time. Nonetheless, the LLS-CUM algorithm entails high computational complexity due to the expanding size of parameter matrices used for location estimation. From our analysis, the LLS-CHLM algorithm emerges as a promising choice, offering a balanced performance trade-off between accuracy and search time with comparatively low computational complexity.

Looking ahead, our future work will examine these algorithms under realistic noise conditions. Moreover, we plan to test the proposed approaches in a real-world UAV testbed, utilizing the emulation and testbed environments of the NSF AERPAW platform at NC State University.

REFERENCES

- [1] Nurbanu Güzey. RF source localization using multiple UAVs through a novel geometrical RSSI approach. *Drones*, 6(12):417, 2022.
- [2] Udit Bhattacherjee, Ismail Guvenc, Ender Ozturk, Mihail L. Sichitiu, Ozgur Ozdemir, and Huaiyu Dai. Experimental study of outdoor UAV localization and tracking using passive RF sensing. In *Proc. ACM Workshop on Wireless Network Testbeds, Experimental evaluation and Characterization (WiNTECH)*. ACM, 2022.
- [3] Du-Hwan Kim, Kyuman Lee, Mun-Young Park, and Jaesung Lim. UAV-based localization scheme for battlefield environments. In *Proc. IEEE Military. Commun. Conf. (MILCOM)*, pages 562–567, 2013.
- [4] Hanguk Lee, Kyuman Lee, and Jaesung Lim. Autonomous maneuvering of relay UAV for battlefields using TDOA localization. In *Proc. IEEE Military. Commun. Conf. (MILCOM)*, pages 748–753, 2017.
- [5] Adrien Perkins, Louis Dressel, Sherman Lo, and Per Enge. Antenna characterization for UAV based GPS jammer localization. In *Proc. ION Int. Tech. Meet. (ITM)*, pages 1684–1695, 2015.
- [6] Dong-Eon Oh and Junghee Han. Smart search system of autonomous flight UAVs for disaster rescue. *Sensors*, 21(20):6810, 2021.
- [7] Muhammad Atif, Rizwan Ahmad, Waqas Ahmad, Liang Zhao, and Joel J. P. C. Rodrigues. UAV-assisted wireless localization for search and rescue. *IEEE Systems Journal*, 15(3):3261, September 2021.
- [8] Sanna Sharafeddine Freddy Demiane and Omar Farhat. An optimized UAV trajectory planning for localization in disaster scenarios. *Computer Networks, J.*, 179(107378):1389–1286, 2020.
- [9] Sara Bernardini, Maria Fox, and Derek Long. *Planning the behaviour of low-cost quadcopters for surveillance missions*, pages 445–453. AAAI Press, 2014.
- [10] Zhongli Liu, Yinjie Chen, Benyuan Liu, Chengyu Cao, and Xinwen Fu. HAWK: An unmanned mini helicopter-based aerial wireless kit for localization. In *Proc. IEEE Int. Conf. Comp. Commun. (INFOCOM)*, pages 2219–2227, 2012.
- [11] Demiane Freddy, Sharafeddine Sanaa, and Farhat Omar. An optimized UAV trajectory planning for localization in disaster scenarios. *Computer Networks*, 179:107378, 2020.

- [12] Imsland. L Albert. A. Combined optimal control and combinatorial optimization for searching and tracking using an unmanned aerial vehicle. *Springer Journal of Intelligent Robotic Systems, J.*, 95:691–706, 2019.
- [13] Matouš Vrba, Jakub Pogram, Václav Pritzl, Vojtěch Spurný, and Martin Saska. Real-time localization of transmission sources using a formation of micro aerial vehicles. In *Proc. IEEE Int. Conf. real-time comp. robot. (RCAR)*, pages 203–208, 2019.
- [14] Udit Bhattacherjee, Ender Ozturk, Ozgur Ozdemir, Ismail Guvenc, Mihail L. Sichitiu, and Huaiyu Dai. Experimental study of outdoor UAV localization and tracking using passive RF sensing. In *Proc. ACM Workshop Wireless. Tetwork. Tesbeds. Eper. eval. cahrac. (WINTECH)*, page 31–38. Association for Computing Machinery, 2021.
- [15] Mehmet Hasanzade, Omer Herekoglu, Ramazan Yeniceri, Emre Koyuncu, and Gokhan Inalhan. RF source localization using unmanned aerial vehicle with particle filter. In *Proc. IEEE Int. Conf. Mech. Aerosp Eng. (ICMAE)*, pages 284–289, 2018.
- [16] Yusuf Said Eroglu, Fatih Erden, and Ismail Guvenc. Adaptive kalman tracking for indoor visible light positioning. In *Proc. IEEE Military. Commun. Conf. (MILCOM)*, pages 331–336, 2019.
- [17] Hasanzade Mehmet, Herekoglu Omer, Yeniceri Ramazan, Koyuncu Emre, and Inalhan Gokhan. RF source localization using unmanned aerial vehicle with particle filter. In *Proc. Int. Conf. on Mechanical and Aerospace Engineering*, 2018.
- [18] B. Liu, X. Zhu, Y. Jiang, Z. Wei, and Y. Huang. UAV and piecewise convex approximation assisted localization with unknown path loss exponents. *IEEE Trans. Veh. Technol.*, 68(12):12396–12400, Dec 2019.
- [19] Ma Maode, Jeong Won Ho, Choi Hong-Rak, and Kim Kyung-Seok. Empirical path loss modeling and a RF detection scheme for various drones. *Wireless Commun. and Mobile Comput.*, 2018:6795931, 2018.
- [20] Priyanka Sinha and Ismail Guvenc. Impact of antenna pattern on TOA based 3d UAV localization using a terrestrial sensor network. *IEEE Trans. Veh. Technol.*, 71(7):7703, 2022.
- [21] Priyanka Sinha, Yavuz Yapici, and Ismail Guvenc. Impact of 3d antenna radiation patterns on TDOA-based wireless localization of uavs. In *Proc. IEEE Conf. Comput. Commun. Workshops (INFOCOM WKSHPS)*, Paris, France, Apr. 2019.
- [22] Shengjun Wu. Illegal radio station localization with UAV-based Q-learning. *China Communications, J.*, 15(12):122–131, 2018.

- [23] Md Moin Uddin Chowdhury, Fatih Erden, and Ismail Guvenc. RSS-Based Q-learning for indoor UAV navigation. In *Proc. IEEE Military. Commun. Conf. (MILCOM)*, pages 121–126, 2019.
- [24] F. Gustafsson and F Gunnarsson. Mobile positioning using wireless networks: possibilities and fundamental limitations based on available wireless network measurements. *IEEE Signal Processing Magazine, J.*, 22(4):41–53, 2005.
- [25] Boda Liu, Xu Zhu, Yufei Jiang, Zhongxiang Wei, and Yi Huang. UAV and piecewise convex approximation assisted localization with unknown path loss exponents. *IEEE Transactions on Vehicular Technology, J.*, 68(12):12396–12400, 2019.
- [26] Kyuwon Han, Seung Min Yu, and Seong-Lyun Kim. Smartphone-based indoor localization using Wi-Fi fine timing measurement. In *Proc. IEEE Int. Conf. Indoor. Posit. Indoor. Nav. (IPIN)*, pages 1–5, 2019.
- [27] Y. Zeng, I. Guvenc, R. Zhang, G. Geraci, and D. W. Matolak. *UAV Communications for 5G and Beyond*. Hoboken, NJ, USA:Wiley, 2020.
- [28] I. Guvenc, S. Gezici, and Z. Sahinoglu. Fundamental limits and improved algorithms for linear least-squares wireless position estimation. *Wireless Communications and Mobile Computing, J.*, (12):1037–1052, 2010.
- [29] H. Li. Low-cost 3D bluetooth indoor positioning with least square. *Wireless Personal Communications, J.*, 78:1331–1344, 2014.
- [30] Mark de Berg and Otfried Cheong. *Computational geometry: Algorithms and applications*, volume 3. Springer, 2008.
- [31] Tauã M. Cabreira, Lisane B. Brisolará, and Paulo R. Ferreira Jr. Survey on coverage path planning with unmanned aerial vehicles. *Drones, J.*, 3(1), 2019.
- [32] S. J. Maeng, O. Ozdemir, I. Guvenc, M. L. Sichitiu, R. Dutta, and M. Mushi. AERIQ: SDR-based LTE I/Q measurement and analysis framework for air-to-ground propagation modeling. In *Proc. IEEE Aerosp. Conf.*, Big Sky, MT, Mar. 2023.
- [33] Sung Joon Maeng, Mrugen A. Deshmukh, Ismail Guvenc, and Arupjyoti Bhuyan. Interference mitigation scheme in 3D topology IoT network with antenna radiation pattern. In *Proc. IEEE Veh. Technol. Conf. (VTC)*, Honolulu, HI, Sep. 2019.
- [34] W.C. Jakes and D.C. Cox. *Microwave mobile communications*. Wiley IEEE press, 1994.
- [35] H. J. Kwon and I. Guvenc. RF signal source search and localization using an autonomous UAV with predefined waypoints. In *Proc. IEEE Veh. Technol. Conf. (VTC)*, June 2023.